Faculty of Physics and Astronomy
University of Heidelberg

Diploma thesis
in Physics

submitted by
Valentin V. Volchkov
born in Novosibirsk, Russia
2009

Cold Lithium Atoms
For Future Polaron Experiments

This diploma thesis has been carried out by Valentin V. Volchkov at the

Kirchhoff Institut für Physik

under the supervision of

Prof. Dr. M. K. Oberthaler

Kalte Lithiumatome für zukünftige Polaron-Experimente

Die vorliegende Diplomarbeit beschreibt einen Aufbau für Experimente mit ultrakalten Gasen aus bosonischem Natrium (^{23}Na) und fermionischem Lithium(^{6}Li). Um die Entartung der Gase zu erreichen, wird Laserkühlung gefolgt von evaporativem und sympathetischen Kühlen angewandt. Die ersten Experimente zielen auf die Untersuchung der Eigenschaften einer Verunreinigung in einem Bose-Einstein Kondensat ab.

Die Bose-Einstein Kondensation von Natrium in einer Magnetfalle wird gezeigt. Ein Lasersystem für das Kühlen und Einfangen von Lithiumatomen in einer magneto-optischen Falle (MOT) wird aufgebaut und in die existierende Apparatur integriert. Die Lithium-MOT wird untersucht und charakterisiert. Innerhalb von zehn Sekunden werden mehrere 10^7 Lithiumatome in der MOT gefangen. Hiervon können einige Prozent in die Magnetfalle transferiert werden. Diese Ergebnisse stellen den ersten Schritt in Richtung von sympathetischem Kühlen mit Natrium dar.

Cold Lithium Atoms For Future Polaron Experiments

This thesis describes a setup for experiments with ultracold gases of bosonic sodium(^{23}Na) and fermionic lithium(^{6}Li). To reach the degeneracy of the gases, laser cooling and subsequently evaporative and sympathetic cooling methods will be applied. In the first experiments one aims to investigate the properties of an impurity immersed in a Bose-Einstein condensate.

Bose-Einstein condensation of sodium in a magnetic trap is performed. A laser system for cooling and trapping of lithium in a magneto-optical trap (MOT) is set up and integrated into the existing apparatus. The performance of the lithium MOT is analyzed and characterized. Within ten seconds, some 10^7 lithium atoms are collected in the MOT, about a few percent of them can be transfered into a magnetic trap. This provides a starting point for the sympathetic cooling with sodium.

Contents

There are two kinds of people, bosons and fermions. And that is not a joke.

A famous russian physicist.

Chapter 1

Introduction

1.1 Polaron Concept

The cartoon depicted in Fig. (1.1) [1] has been used to explain politicians how the Higgs mechanism is supposed to work. The people at the cocktail party are evenly distributed and talk to their neighbours. They represent the Higgs-field. A famous person tries to cross the room, but immediately attracts other people as soon as she gets close to them.

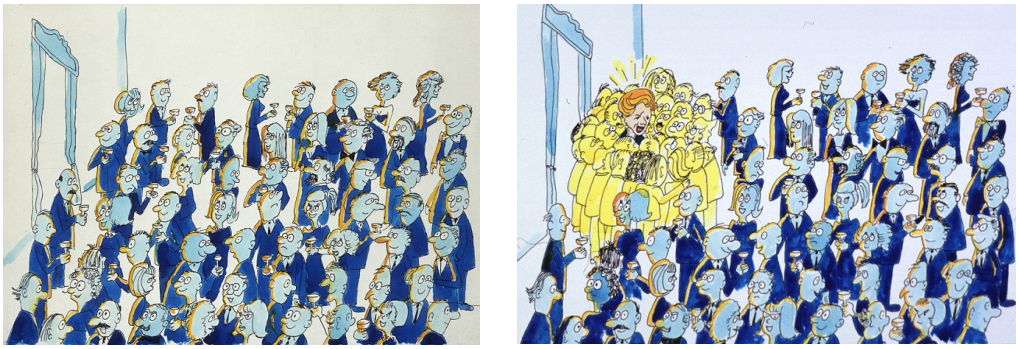

Figure 1.1: The Higgs mechanisms for dummies. On the left, the background Higgs field is represented by the party society. A particle moving in the field acquires mass by interacting with the people in the room.

Dragging the cluster of excited people along the way gives the famous person mass. Eventually, the excited people return to their original positions (and conversation) after the famous person has passed. Although this cartoon was intended to make the government raise funds for Higgs research, it also illustrates a very general concept of a quasi-particle called *polaron*. Author David J. Miller explained to the UK Science Minister:

> ... The idea comes directly from the Physics of Solids. Instead of a field spread throughout all space a solid contains a lattice of positively charged crystal atoms. When an electron moves through the lattice the atoms are attracted to it, causing the electron's effective mass to be as much as 40 times bigger than the mass of a free electron.

Without naming it, he talks about the standard example of a polaron: an electron that polarizes the lattice of ions via the Coulomb interaction. In that case, the excitations of the lattice following the electron are phonons.

In general terms, a particle moving through a medium and interacting with it can be described as a new quasi-particle with new properties and a different effective mass. In the case of the cartoon, the fact that the people are talking to their neighbours is very important, in this way a local distortion in one corner of the room actually affects the whole medium. This concept is very fundamental, since it can be applied to completely different systems with different interaction strengths.

Polarons in solids may provide the key to understanding of mechanisms such as high-T_C superconductivity or colossal magnetoresistance. Open theoretical questions are the properties of polarons at strong coupling constants, for which Monte-Carlo simulations differ from analytical approaches.

1.2 Ultracold Quantum Gases

The motivation for the experiment described in this thesis is to implement a model system for polarons using ultracold gases.

The success of laser cooling followed by evaporative cooling led to first experimental realization of Bose-Einstein condensation in 1995 and opened a new field in atomic physics [2, 3, 4]. Many fundamental effects of quantum mechanics like the tunneling effect or the interference of wavepackets could be realized on a macroscopical scale using Bose-Einstein condensates (BEC) formed of dilute alkali gases [5, 6]. Phenomena of superfluidity could be reproduced and studied in a pure form without the complications of strong interactions of liquid Helium. Placing a BEC in a periodic potential created by an optical lattice gave birth to an additional class of systems, mimicking physics in solids. The transition from a normal to a Mott-insulating state thus could be investigated by controlling the parameters of the periodic potential [7]. The discovery of Feshbach-resonances for atoms allowed for tuning of the interactions between the atoms [8]. Attractive interaction between ultracold fermions generated pairs of fermions with different spins [9, 10]. These pairs are analogues to the well known Cooper-pairs in solids

which are described by the theory of Bardeen, Cooper and Schrieffer(BCS) in which Cooper-pairs of electrons are responsible for the phenomenon of superconductivity [11].

The advantages of systems made out of ultracold gases are the low temperatures that could not be reached in other systems, the almost perfect isolation from the outer world and the full control of relevant parameters.

So far, polaronic behavior in ultracold gases has been observed in a Fermi-Fermi mixture [12] and in Bose-Fermi mixtures by Ref.[13, 14]. We are going to use a BEC as the medium for fermionic impurities.

1.3 Polarons in a Bose-Einstein condensate

There are several good reasons to use a condensate as a medium for polarons, which we review now.

1.3.1 Bogoliubov excitations

The first is the similarity of physical systems. It is not evident what an electron on a lattice has in common with a fermionic atom immersed in a BEC. Therefore, we should take a closer look at the properties of a Bose-Einstein condensate.

In a gas of non-interacting bosons all of them occupy the ground state at zero temperature [15]. If we turn on weak (repulsive) interactions, the total energy can be minimized by populating low excited states, thereby reducing the total interaction energy of the gas. The fact that even at $T = 0$ a fraction of atoms is excited due to the interactions is called quantum depletion. The interaction energy itself depends on the occupation of different excited states and the occupation of excited states depends on the interaction energy, turning the situation to a complex many-body problem. In other words, the behavior of each particle [1] depends on all other particles and we cannot describe the particles independently. Therefore, it is very inconvenient to view the condensate just as a number of bosonic atoms. Hence, we will consider it from another perspective: we take the gas as it is, containing many atoms in the 'non-interacting' ground state and a few in excited states and define this as the *new* ground state of the system. In technical terms, we perform a transformation by diagonalizing the Hamiltonian. The Bogoliubov transformation yields a system with a positive ground state energy (which is not surprising since we have repulsive interactions) and a dispersion law $\epsilon(p)$ for the elementary excitations of the system [17]. Elementary excitation means

[1] The behavior corresponds basically to the state which it occupies.

that whenever our system gets a kick, we ignore what happens to real atoms, instead we describe it by creating independent quasi-particles with certain momentum and energy. How much energy a quasi-particle gets for a given momentum is determined by its dispersion law. The dispersion law $\epsilon(p)$ is the amount of kinetic energy of an excitation as a function of momentum and contains all important properties of our system. In the case of the Bogoliubov transformation, it states that for high momenta, the energy depends on the square of the momentum exactly as for free particles. [2] However, for low momenta the energy scales linearly with the momentum which corresponds to phonon-like excitations.

This is the point where we meet the physics of solids. Introducing an impurity into the BEC will locally disturb the BEC, analogously to the distortion of an ion lattice by an unbound electron. In both cases, the local distortion can be described by creating appropriate phonons. Again, we can perform a transformation and define the impurity with the phonons as a new quasi-particle, the *polaron*.

This transformation and the resulting properties of the polarons are nontrivial. Especially the properties depend on the type and strength of interactions between the impurity and the medium. For electrons-phonon interactions the strength is expressed by a coupling constant α and depends on the materials. As a matter of fact, for large values of α, different theoretical approaches to obtain the properties of polarons give different predictions and do not agree with the numerical simulations. Unfortunately, no materials are known to have coupling constants for the strong coupling regime.

1.3.2 Interaction strength

This brings us directly to the second good reason for modeling polarons with BECs. The coupling constant for an impurity in a BEC has the following form: $\alpha \propto a_{\mathrm{IB}}^2/a_{\mathrm{BB}}$, where a_{BB} is the scattering length[3] between bosons and bosons, and a_{IB} is the scattering length between impurity and bosons [18]. The given form for α makes perfectly sense, the effect of distortion is larger with stronger interactions between bosons and the impurity. On the other hand, strong interactions among bosons oppose the distortion. The advantage of the polarons in BEC is that the coupling constant is not a constant fixed by the material as it is in solids, but can be tuned via inter-species Feshbach-resonances[13, 14, 19]. Realizing polarons at different couplings could lead to the test of theories in the challenging regime.

[2] That is, for large p it is of the form: $\epsilon(p) \approx \frac{p^2}{2m} + const.$

[3] The interaction strength is proportional scattering length.

1.3.3 Mean-field description

The third argument for using BECs as a medium stems from the mean-field description of the dynamics in the condensate. The evolution of the wave-function $\Psi_{\mathrm{I}}(\vec{r},t)$ of the impurity is given by the Schrödinger equation with an additional term that accounts for the interaction between the impurity and the condensate.

$$i\hbar\frac{\partial}{\partial t}\Psi_{\mathrm{I}}(\vec{r},t)=\left(-\frac{\hbar^2\nabla^2}{2m_{\mathrm{I}}}+\underbrace{V_{\mathrm{ext}}(\vec{r},t)+g_{\mathrm{IB}}\left|\Psi_{\mathrm{B}}(\vec{r},t)\right|^2}_{\text{Effective potential}}\right)\Psi_{\mathrm{I}}(\vec{r},t) \tag{1.1}$$

where $V_{\mathrm{ext}}(\vec{r},t)$ is an external potential and $g_{\mathrm{IB}}=\frac{4\pi\hbar^2 a_{\mathrm{IB}}}{m}$ is the interaction strength between the impurity and the bosons.The major advantage of the mean-field approach is that the condensate itself can be approximated by a single order parameter $\Psi_{\mathrm{B}}(\vec{r},t)$ that obeys the Gross-Pitaevskii equation (GPE) [17]:

$$i\hbar\frac{\partial}{\partial t}\Psi_{\mathrm{B}}(\vec{r},t)=\left(-\frac{\hbar^2\nabla^2}{2m_{\mathrm{B}}}+V'_{\mathrm{ext}}(\vec{r},t)+g_{\mathrm{BB}}\left|\Psi_{\mathrm{B}}(\vec{r},t)\right|^2\right)\Psi_{\mathrm{B}}(\vec{r},t) \tag{1.2}$$

By adding the term $g_{\mathrm{IB}}\left|\Psi_{\mathrm{I}}(\vec{r},t)\right|^2$ into the brackets of the right hand side of Eq.(1.2), we get two coupled differential equations for Ψ_{B} and Ψ_{I}, which can be solved numerically in a self-consistent way. Experimentally accessible quantities are spatial distributions of the atoms and their temporal behavior. Both can be directly obtained from the solutions for Ψ_{B} and Ψ_{I}.[4] Thus, predictions for different trapping potentials and interaction strengths can be made and verified in the experiment. In Ref.[18, 20] ground states for impurities in a background BEC have been computed, indicating a sudden localization for a critical interaction strength. It is also interesting to see at which point the mean-field description breaks down.

1.4 The Experiment

The primary goal of the NaLi experiment is to investigate polaronic behavior of impurities immersed in a Bose-Einstein condensate. Bosonic sodium (^{23}Na) and fermionic lithium (^{6}Li) are simultaneously cooled until the degeneracy of sodium is reached. Both species are transfered in a large volume optical trap. An additional trapping potential for lithium allows for extra

[4] The density of the condensate can be obtained from the order parameter using: $n_B(r,t)=\left|\Psi_{\mathrm{B}}(r,t)\right|^2$.

control over localization of lithium within the BEC, as illustrated in Fig.(1.2) [21]. A homogeneous magnetic field enables us to tune the interactions via Feshbach resonances between sodium/sodium and sodium/lithium. In first experiments we will measure the oscillations of lithium in its trap and thus the effective mass depending on the interaction strength.

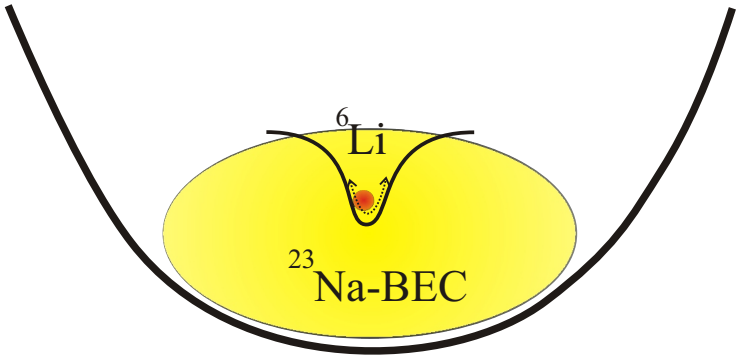

Figure 1.2: Illustration of polaron experiment: Oscillating fermions will acquire a larger effective mass due to interaction with the background BEC.

Apart from polarons, all kinds of experiments proposed for Bose-Fermi mixtures can be realized with our setup.

1.5 Outline of this thesis

The present thesis reports on the preparation of the ultracold gases for the polaron experiments. In the case of sodium, we demonstrate evaporative cooling below 10 μK and first signs of Bose-Einstein condensation. The main emphasis of the thesis lies on the magneto-optical trapping of lithium. The optical setup for laser cooling of lithium is explained in details. Furthermore, lithium atoms in the magneto-optical trap are characterized. The compression of the lithium MOT and the transfer of lithium into the magnetic trap are tempted. Eventually, the last steps towards the polarons are summarized in the outlook of this thesis.

Chapter 2

Sodium, the medium

So welcome to the machine.
Pink Floyd

Bose-Einstein condensation of dilute alkali gases occurs at temperatures around 1 μK. Starting from a thermal gas, we have reduce the temperature by 8 orders of magnitude. At the same time, the density has to be increased to 10^{14} atoms/cm^3 to obtain a Bose-Einstein condensate (BEC), that will act as the medium for the polarons. The first purpose of this chapter is to introduce the techniques used for cooling both sodium and lithium. The second aim is to get known to the experimental realization of these techniques for sodium. Evaporative cooling will be used to demonstrate the capability of reaching ultracold temperatures for sodium. Absorption imaging will prove as a useful analytical tool.

2.1 Laser Cooling

Over the past decades laser cooling has become a powerful and very commonly used tool in atomic physics. In this section, basic principles of laser cooling will be briefly discussed, providing the physical quantities, necessary for the implementation of this technique in our experiment. A more complete and thorough description can be found in Ref.[23].

Laser cooling of atomic gases is actually laser *slowing*, since the temperature of a (classic) gas at thermal equilibrium is proportional to the square of the mean velocity and is given by: $mv^2/2 = 3k_BT/2$. Therefore, reducing the velocity is equivalent to reducing the temperature.

The concept of laser cooling relies on interaction of atoms with (laser)light. In a simple picture, an atom can be considered a two-level system. The two

levels correspond to the ground and excited electron states and are separated by the energy of $\hbar\omega_0$. Obviously, the atom can be excited from the ground state by absorbing a photon (with an energy) $\hbar\omega_0$, at the same time the atom receives a recoil momentum $\Delta p = \hbar k$. The lifetime τ of the excited state defines the maximum scattering rate $\gamma \propto 1/\tau$.

The whole cooling mechanism presented in the following works basically due to the fact that the spontaneous emission of the photons and the recoil go in a random direction whereas all absorbed photons come from the same direction. This results in a net force (in the propagation direction of the light), that can be used to slow (or accelerate) and thus cool (heat) atoms. This force is known as the spontaneous or pressure force. A very simple and intuitive picture of this slowing is given in Fig. (2.1).

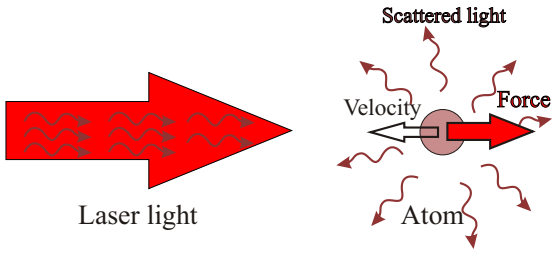

Figure 2.1: An atom moves at a certain velocity, while laser light comes from the opposite direction. The scattering of photons gives rise to a net force directed along the laser light. The reemission of photons is isotropic.

2.1.1 Spontaneous force

As already mentioned, the spontaneous force relies on scattering of photons. The force can be written as the product of the transfered momentum Δp and the scattering rate γ:

$$F_{\mathrm{S}} = \Delta p \gamma = \hbar k \gamma \tag{2.1}$$

In general, the scattering rate depends on the detuning $\delta_0 = \omega - \omega_0$ of the laser frequency ω with respect to the atomic transition frequency ω_0 and on the intensity of the light[23]:

$$\gamma = \frac{\Gamma}{2} \frac{s_0}{1 + s_0 + (2\delta/\Gamma)^2} \tag{2.2}$$

The intensity enters the scattering force in units of saturation intensity I_{S} through the saturation parameter $s_0 = I/I_{\mathrm{S}}$. We immediately see that

increasing the intensity $I \gg I_S$ leads to a saturation of γ at $\Gamma/2$, Γ being the natural line width of the transition. For large detunings $\delta \gg \Gamma$ the spontaneous force vanishes. The irreversible nature of spontaneous emission makes this force a dissipative one and therefore suitable for cooling.

Our goal is to slow atoms using the scattering force. For moving atoms the velocity dependence of F_S enters in the detuning: an additional frequency shift of $\delta_{\text{Doppler}} = kv$ arises from the Doppler effect ($k = 2\pi/\lambda$), leading to a total detuning of: $\delta = \delta_0 + \delta_{\text{Doppler}}$.[1]

Applications

The introduced principles can be directly applied in the experiment. The simplest application of the spontaneous force that can be thought of would be shining laser light on incoming atoms, like shown in Fig.(2.1). Lithium or sodium atoms coming from an oven at 400°C have velocities around 1000 m/s, corresponding to a Doppler shift of $2\pi \times 1.5$ GHz. The detuning of the laser can be chosen such that it cancels out the Doppler shift, making the light resonant to the fast atoms. Theoretically, as long as the atoms move towards the light, they are decelerated, though the limitation of this cooling technique is obvious: while slowing the atoms, due to a changing Doppler shift, the spontaneous force brings them out of resonance and tends to zero for increasing detuning. This slowing technique cuts a hole into the Maxwell-Boltzmann distribution for the resonant velocity and increases slightly the atom flux at the velocity below the resonant one. Even if this slowing is a very inefficient one, by choosing a relatively small detuning of $- \approx 2\pi \times 100$ MHz one still can pre-cool a small fraction of atoms preparing them for further cooling steps[24].

Zeeman Slower

A far more powerful and efficient slowing can be achieved by keeping the atoms on resonance over larger range [25]. In our experiment we have implemented a so-called Zeeman slower [26]. In order to keep the atoms on resonance at all times, a spatially varying magnetic field $\vec{B}(x)$ is applied.

[1] In general, we have $\delta_{\text{Doppler}} = -\vec{k}\vec{v}$, for a laser beam counterpropagating in respect to the atom we obtain: $\delta_{\text{Doppler}} = kv$

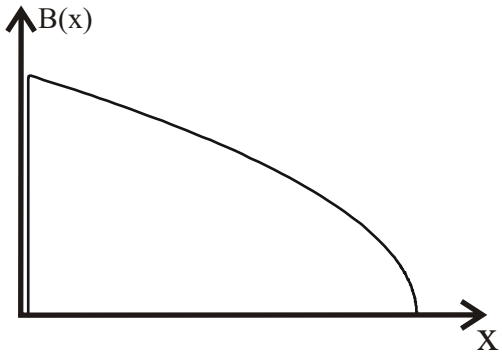

Figure 2.2: Inhomogeneous magnetic field to compensate for the changing Doppler shift.

An atom with a magnetic moment $\vec{\mu}$ experiences the Zeeman effect when an external magnetic field is present. The energy shift of the level is given by $\Delta E_Z = \Delta\vec{\mu}\vec{B}(x)$.[2] Due to different magnetic moments of ground and excited states an extra term can be added to the overall detuning:

$$\delta = \delta_0 + \delta_{\text{Doppler}} + \frac{\Delta\vec{\mu}\vec{B}(x)}{\hbar} \tag{2.3}$$

The Zeeman slower is an elongated solenoid that makes sure that over its length the scattering force stays maximal ($\delta = 0$), by producing a Zeeman shift that compensates for the changing Doppler shift. The final velocity can be adjusted with the magnitude of the magnetic field and the detuning of the laser. Usually, $v_{\text{final}} = 30 - 50\,\text{m/s}$ is slow enough for further cooling steps.

2.1.2 Optical molasses

For velocities around 30 m/s the Doppler shift is $\delta_{\text{Doppler}} = 2\pi\times(30-40\,\text{MHz})$, which comes close to the natural transition line width. If we again use one beam with detuning $\delta_0 = -\delta_{\text{Doppler}}$, the atom comes to rest, but is then accelerated back where it came from, see Fig. (2.3,a). What we need in order to *keep* the atom at rest is a force that is always opposed to the velocity (therefore always a slowing one) and equals zero for $v = 0$, analogous to Stokes' Law. Two red-detuned, counterpropagating laser beams result in the desired force.[3] This configuration is called optical molasses (OM) and is illustrated in Fig. (2.3,b). The total force can be written as the sum of two

[2] For a description of atoms in external fields refer to standard textbooks like [27].
[3] All effects arising from interference of beams are neglected.

forces:

$$F_{\mathrm{OM}} = \hbar k \frac{\Gamma}{2} \left(\frac{s_0}{1 + s_0 + (2(\delta_0 - kv)/\Gamma)^2} - \frac{s_0}{1 + s_0 + (2(\delta_0 + kv)/\Gamma)^2} \right) \quad (2.4)$$

A first order Taylor expansion leads to:

$$F_{OM} = -\beta v \quad (2.5)$$

where β is a positive friction coefficient.

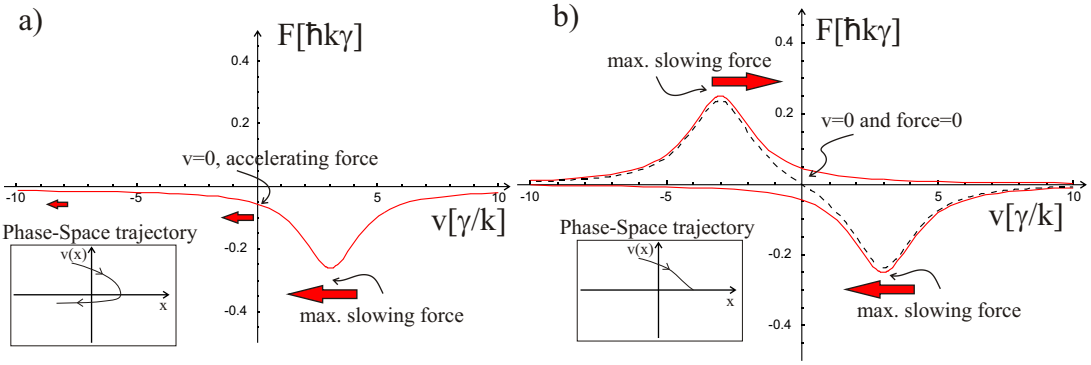

Figure 2.3: In a), a single red-detuned laser slows the atom until its motion is reversed, as shown in the phase-space diagram. An optical molasses consists of two counterpropagating laser beams, the scattering force of both beams adds up as shown in b)(dashed line). The force vanishes for $v = 0$. The atom is trapped in velocity space, while its position is arbitrary.

An optical molasses, consisting of two pairs of orthogonally crossing laser beams, can be used to collimate a divergent atom beam by damping out its transversal velocity component.

Overlapping three pairs of counterpropagating beams leads to a region where incoming atoms experience a velocity-dependent friction in all directions and slow down. Using this so-called Doppler cooling method, one can achieve temperatures as low as a few hundred μK. A heating rate, arising from a random walk in momentum space sets a limit for the lowest possible Doppler temperatures. The temperature as a function of detuning is given by [23]:

$$T(\delta_0) = \frac{\hbar\Gamma}{4k_B} \frac{(2\delta_0/\Gamma)^2 + 1}{|2\delta_0/\Gamma|} \quad (2.6)$$

and has a minimum temperature T_{D} for $\delta_0 = -\Gamma/2$, as shown in Fig.(2.4).

$$T_D = \frac{\hbar\Gamma}{2k_{\mathrm{B}}} \quad (2.7)$$

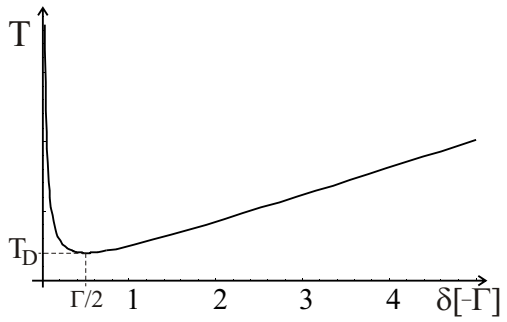

Figure 2.4: Temperature of atoms in an optical molasses depending on the detuning of the laser beams.

2.1.3 Magneto-Optical Trapping

The scattering force and optical molasses allow us to cool atoms below 1 mK. Cold atoms still can leave the OM due to their minimum velocity corresponding to the Doppler temperature and the lack of a spatial confinement. To create a confinement in space we need a restoring force towards the center, analogous to Hooke's Law $F = -\alpha x$, where α is a positive spring constant. Similar to optical molasses (2.5), but now in position space, we want an atom to scatter light only from one of the beams depending on where it is.

So far, a simple two-level scheme of an atom was enough to understand the principles of laser cooling. Nonetheless, real atoms have complicated transition schemes that obey selection rules for different polarizations. We are going to use these selection rules to establish a restoring force in space. Let us consider an atom with angular momentum $F = 0$ in the ground state. When the counterpropagating beams of the OM have opposite circular polarization, σ^+-polarized light excites the atom into $m_\mathrm{F} = +1$ state and vice versa, but since the sub-states are degenerated without an external magnetic field, we get neither position dependent force nor a selectivity of the exciting light. Adding a linear magnetic field $B(x) = B'x$, with B' being the magnetic field gradient (usually, in the order of $10 - 20\,\mathrm{G/cm}$), leads to a position-dependent detuning (see paragraph(2.3)) and therefore a position-dependent force. At the same time, the energy of the m_F-states of the excited state is split up due to different magnetic moments and provides the selectivity, see Fig.(2.5). An atom traveling in $x > 0$ space is more likely to be excited into the $m_\mathrm{F} = -1$ state by absorbing a photon from the σ^- beam and is thus driven towards the origin. While the restoring force creates an effective potential and confinement around $B = 0$, the light force damps out (cool)

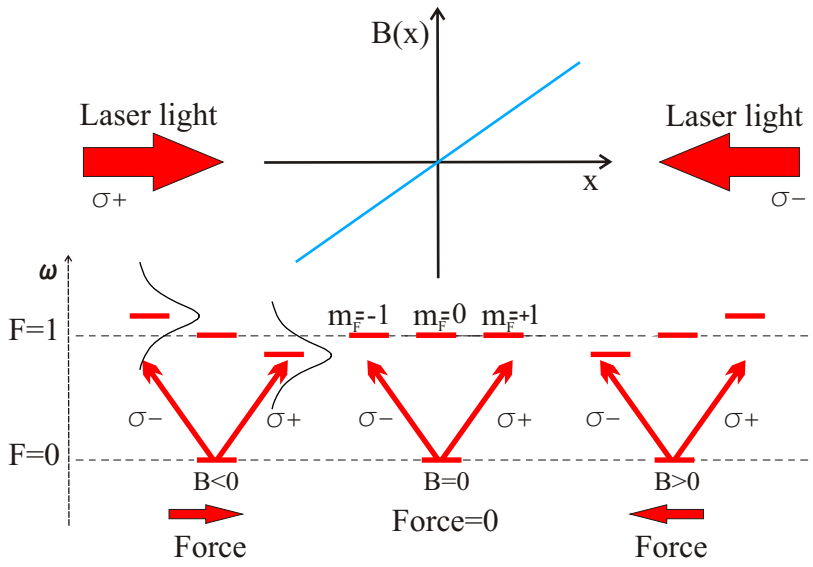

Figure 2.5: Magneto optical trapping: restoring force arises due to an inhomogeneous magnetic field B(x) and selection rules for circularly polarized light. For $B < 0$, profiles of the scattering rate are indicated, the width depends on the gradient of the magnetic field. (Scheme was adopted from [26].)

the motion of the atoms.

A Magneto Optical Trap (MOT) is therefore a combination of an optical molasses and an inhomogeneous magnetic field that allows for cooling and trapping of the atoms [28]. For small velocities and close to the center, the force acting on atoms in a MOT is now a sum of a restoring force in momentum space Eq.(2.5) and a restoring force in position space:

$$F_{MOT} = -\beta v - \alpha x \tag{2.8}$$

A good working MOT is crucial for all following cooling stages. The number of atoms and their temperature determine the success of the whole experiment.

Characteristics

The figures of merit of a MOT are the *atom number* and the *loading rate*. The maximum atom number in a MOT is directly proportional to the loading rate. The loading process mainly depends on two factors: it is proportional to the flux of cold atoms and therefore relies on a good working Zeeman slower. The second factor is the efficiency of trapping of the slowed atoms in

the MOT. Clearly, these properties of the MOT depend on the detuning and intensity of the trapping light and the gradient of the magnetic field. The interplay of these parameters can be summarized in following factors: MOT potential and capture range/velocity.

MOT potential and capture range

Generally, the force in a MOT can be written as:

$$F_{OM} = \hbar k \frac{\Gamma}{2} \left(\frac{s_0}{1 + s_0 + (2(\delta_+/\Gamma)^2} - \frac{s_0}{1 + s_0 + (2(\delta_-/\Gamma)^2} \right) \tag{2.9}$$

with the detuning $\delta_\pm = \delta_0 \pm kv \pm \Delta\mu B' x/\hbar$. Integration along x in one dimension, yields for $v = 0$ a potential[4] that is seen by the atoms at rest as illustrated in Fig.(2.6,a). For large detunings $\delta \gg \Gamma$ and high magnetic field gradients, the potential has a box-like shape with a width about twice the capture range:

$$r_c = \frac{\hbar\delta_0}{\Delta\mu B'} \tag{2.10}$$

The capture range gives the distance from the trap center at which slow atoms are in resonance (assuming a negligible Doppler shift) with the laser light. The capture range determines the volume (given by the potential) of the MOT and the trapping area. Therefore, a large capture range allows for capturing atoms even from a divergent atom beam, thus increasing the loading rate.

Capture Velocity

The velocity of atoms that can be stopped just before leaving the trapping region is denoted by the capture velocity v_c. In order to trap the atoms from the Zeeman slowed atomic beam, v_c should be larger than the final velocity of the incoming atoms. An optimistic estimate can be obtained by assuming $F = \hbar k\Gamma/2$ over the diameter of MOT beams, giving $v_\mathrm{c} \approx 100\,\mathrm{m/s}$ [23]. A more accurate way to determine v_c is solving the equation of motion numerically with Eq. (2.9) for different velocities and results in $v_\mathrm{c} \approx 30-40\,\mathrm{m/s}$[26]. Obviously, a larger detuning allows for a higher Doppler shift and thus raises the capture velocity. Numerical simulations show that v_c drops for detunings $\delta_0 < -10\Gamma$, this corresponds to the case when the

[4]Since the scattering force is not conservative, no representation as potential is possible. To illustrate the working principle of a MOT, the integration was performed by omitting the velocity dependence.

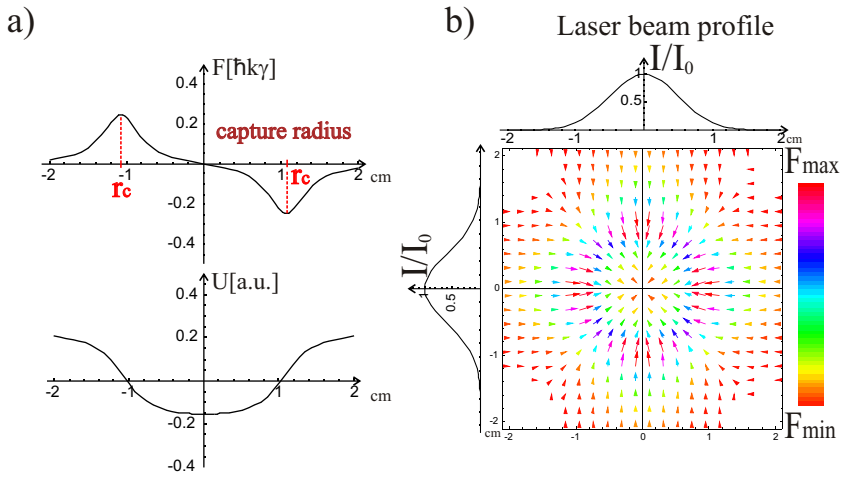

Figure 2.6: Forces and 'potentials' seen by an atom at rest. The integration was performed with $v = 0$ for all positions. In a) the scattering force and the corresponding potential are plotted for $s_0 = 1$, $\Gamma = 2\pi \times 6\,\mathrm{MHz}$, $B' = 10\,\mathrm{G/cm}$ and a detuning $\delta_0 = -2\pi \times 15\,\mathrm{MHz}$. The vector field in b) illustrates the scattering force from four beams (2D-MOT). The finite size of the laser beam, denoted by the gaussian intensity profile, has been taken into account. The area in the center is surrounded by restoring forces.

detuning is too large for small velocities and atoms are out of resonance before they get stopped.

Dynamics of the MOT

The temporal behavior of the MOT can be described as a steady competition of loading and loss processes. The loss rate has several contributions that can be summed up to one- and two-body losses[5] [29].

$$\frac{dN}{dt} = L - 1/\tau N - \beta N^2/V \tag{2.11}$$

where the loading rate L[atoms/s] is the flux of atoms being trapped in the MOT. One-body losses occur due to collisions with the background gas and misalignment of the MOT beams, which leads to a leaky MOT potential. Because of their independent nature, the one-body loss coefficient $1/\tau$ does

[5]Three-body losses become important only at densities that are not achievable in a MOT.

not depend on the total atom number N. Two-body loss rate involves the proximity of two atoms, therefore depends on the density $\propto N/V$ of atoms, with β as the two-body loss coefficient.

Among others, there are two important two-body loss channels, being the radiative escape and the fine-structure change [30]. Both cases involve the interaction of two atoms, one of them being in the excited state. Radiative escape may occur when an excited atom is accelerated in a long-range potential created with the other atom. The kinetic energy gained may suffice to leave the trap. A loss from the trap is also possible when the excited atom changes its fine structure state from $P_{3/2}$ to $P_{1/2}$ during a collision with another atom, sharing the gained energy with the collision partner. In order to limit the two-body losses, one can reduce the scattering rate and by that limit the population in the excited state.

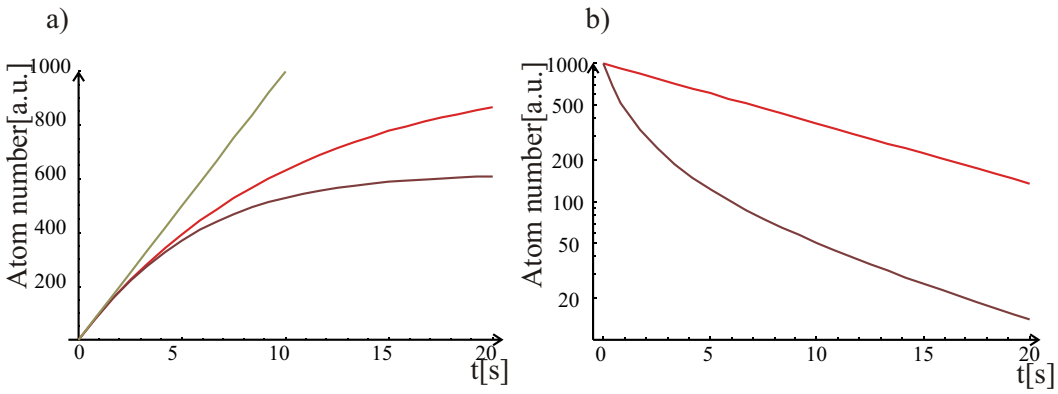

Figure 2.7: Fig. a) Shows loading curves with the same loading rate. While all three curves are linear in the origin, one and two body-losses lead to saturation. The decay curves give information on contribution of loss rates.

Fig.(2.7,a) shows different loading curves, for low atom numbers the growth is linear; when the one-body losses increase, the loading curve begins to saturate like $N(t) = N_0(1 - e^{-t/\tau})$; saturation is reached when the loading rate equals the losses. If one switches off the loading of the trap, the decay of the MOT shown in Fig.(2.7,b) is exponential when the two body losses are neglected. In the case of high two-body losses, the number of atoms is given by Eq.(2.12). The decay is stronger than exponential in the density limited regime. At low atom numbers, the two-body losses tend to zero and the decay becomes exponential.

$$N(t) = \frac{N_0 e^{-t/\tau}}{1 + N_0 \tau \beta (1 - e^{-t/\tau})} \tag{2.12}$$

Laser cooling of sodium

The principle of laser cooling relies on the availability of a closed transition, hence on the validity of the two-level model approximation. However, hyperfine coupling of the spin-orbit and nuclear spins, leads to a hyperfine structure with level spacings in the order of several MHz to several GHz for alkali atoms. Real atoms therefore are multi-level systems, which allows them to escape from a closed transition with some probability.

In case of sodium, we use the $F = 2, m_{\mathrm{F}} = \pm 2 \rightarrow F' = 3, m_{\mathrm{F}'} = \pm 3$ transitions with $\sigma^{\pm}$ -light as two-level system. Nevertheless, excitation into the $F' = 2$ states may occur due to the finite level spacing, decay into the untrapped $F = 1$ ground state is then no longer forbidden. To close this loss channel, an additional beam called repumper optically pumps the atoms back into the $F = 2$ state using the $F = 1 \rightarrow F' = 2$ transition, as shown in Fig. (2.8).

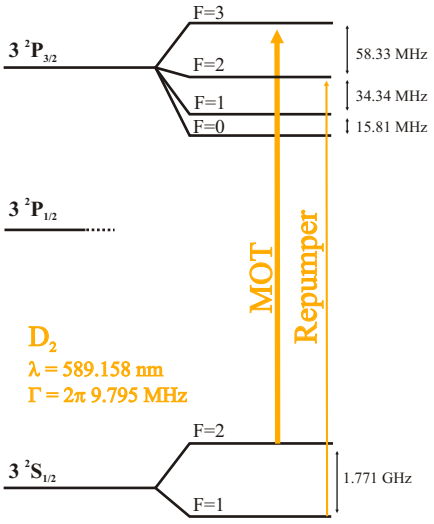

Figure 2.8: Transitions used for magneto optical trapping of sodium. The MOT-light cools and traps atoms with the $F = 2, m_{\mathrm{F}} = \pm 2 \rightarrow F' = 3, m'_{\mathrm{F}} = \pm 3$ transition. Atoms fallen into the dark $F = 1$ state are pumped back into the cycling transition with the repumper light.

Particularities of laser cooling of lithium will be discussed in section (3.1).

2.2 Cooling strategy and the experimental setup

To reach ultra low temperatures in our experiment several cooling steps are necessary. The pre-cooling stage makes use of the laser cooling techniques we saw in the previous sections. The source of atoms is an effusive oven. The hot vapor leaves the oven at temperatures of 700-800K. A Zeeman slower decelerates the atoms to velocities around 40 m/s corresponding to 1K. The slow atoms are captured by a MOT where they are further cooled to temperatures below 1 mK. The density of our atomic sample in the MOT does not exceed 10^{11} atoms/cm^3. To compress the atoms, they are transfered into a conservative potential of a magnetic trap (MT), where they are subsequently evaporatively cooled to reach final temperatures in the order of 1 μK.

Evaporative and sympathetic cooling

In principle, the first cooling stages, relying on laser cooling, that is Zeeman slowing and magneto-optical trapping, are identical for sodium and lithium. However, evaporative cooling in the magnetic trap works only for sodium. The evaporative cooling bases on reaching of the thermal equilibrium after hot atoms are removed from the sample; the new temperature is then below the original one. This process of thermalisation is sustained by collisional relaxation. Collisions at low temperatures are reduced to s-wave scattering, but Pauli principle forbids s-wave scattering of identical fermions. A spin polarized sample of indistinguishable lithium-6 atoms does not thermalise as the elastic collision rate diminishes proportionally to T^2 [31]. In our case this does not present a problem, since transferring lithium and sodium into the same magnetic trap ensures thermal equilibrium between the two species [32]. Hence, evaporative cooling of sodium means simultaneous sympathetic cooling of lithium.

Experimental realization

The following part describes briefly the implementation of the cooling strategy and the necessary technical framework. The implementation of laser cooling for lithium will be discussed separately and in greater detail in section 3.1.

Vacuum

While talking about experiments in the sub-mK range, naturally the question arises of how to isolate the system from the outer world at room temperature. The commonly used approach is to prepare the system in a vacuum

environment. In our case, the experiment will take place in a glass cell at ultra high vacuum (UHV) with pressure well below 10^{-10} mbar. The pressure of the background gas defines the heating rate, as it basically conducts the heat from the walls of the glass cell to the atoms. On the other side, we want a high flux of cold atoms, which requires a high partial pressure of sodium and lithium in the oven. The challenge is to achieve both, high atomic flux and UHV, in one setup.

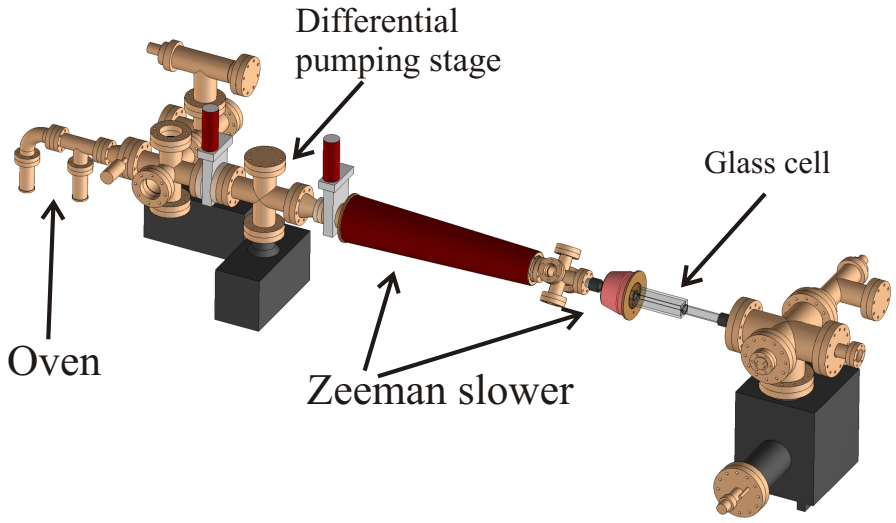

Figure 2.9: Overview on the experimental chamber. Figure taken from [33].

This is done by dividing the setup into several chambers with gradually decreasing pressure. The partial pressure of lithium and sodium in the oven amounts up to $10^{-1} - 10^{-3}$ mbar depending on the temperature of the oven. The atoms diffuse via a nozzle into the oven chamber. An atomic beam is formed by aligning the oven nozzle with a 5 mm large aperture. An ion getter pump reduces the pressure in the oven chamber to 10^{-8}mbar. A shutter inside the oven chamber can be used to block the atomic beam. The atomic beam subsequently enters into the next chamber via a 130 mm long conical tube. This chamber, denoted as the differential pumping stage, has a pressure two orders of magnitude lower than in the oven chamber. The Zeeman slower and the glass cell present the final chamber. The slower is connected to the differential pump via an other tube, which decreases the pressure by another factor of 10. The oven nozzle, the collimating aperture as well as the differential pumping tubes and the slower are aligned in such

a way, that atoms can travel directly from the oven to the glass cell. Finally, the glass cell is connected to a titanium sublimation pump, producing a pressure of 10^{-11}mbar. A detailed description of the vacuum setup is given in the diploma thesis of Marc Repp [33].

Zeeman slower

The atoms enter the Zeeman slower with an average velocity of 800m/s (for sodium) and 1600m/s (for lithium). The goal is to slow a reasonable fraction of them to around $30 - 50$m/s. The principle of function of the slower is given in section 2.1.1.

Assuming, that the deceleration is given by: $a_{\max} = \frac{\hbar k \Gamma}{2m}$, the resonance condition ($\delta = 0$) yields the following equation for the shape of the magnetic field[26]:

$$B(x) = B_0 \sqrt{1 - \frac{x}{L}} + B_{\text{Offset}} \tag{2.13}$$

B_0 determines the "velocity range" $v_{\max} - v_{\text{final}}$, that is, the difference between the maximal velocity that can be slowed and the final velocity. Due to a finite deceleration $a_{\max}$ the minimal length L of the slower is given by:

$$L = \frac{v_{\max}^2 - v_{\text{final}}^2}{2a_{\max}} \tag{2.14}$$

The final velocity is reached for $x = L$ and can be extracted from the resonance condition, $\delta_0 + k v_{\text{final}} + \frac{\Delta \mu B_{\text{Offset}}}{\hbar} = 0$. The choice of the detuning δ_0 and B_{Offset} defines the final velocity.

The maximum deceleration $a_{\max} = \frac{\hbar k \Gamma}{2m}$ requires an intensity that is much higher than the saturation intensity. Laser power limitation leads to a smaller deceleration, therefore the length of the slower (2.14) has to be increased.

The magnetic field created by a real solenoid always has imperfections and deviations from the calculated shape in Eq.(2.13). It means, that if at some point along the slowing trajectory the resonance condition is not fulfilled due to an abrupt change of the magnetic field, the atoms may leave the slowing process and never reenter. This can happen when the gradient of the field is too steep. To circumvent this loss, the length should be chosen larger than necessary according to Eq.(2.14).

An important criterion is the detuning of the slowing laser beam. On the one hand, the slowing beam should not be in resonance with atoms in the MOT, on the other hand the detuning cannot be chosen arbitrarily large since this would require a high offset field B_{Offset}, which would perturb the field of the MOT.

The resulting design for the Zeeman slower corresponds to a so-called zero-crossing configuration with $B_0 = 800G$ and $B_{\text{Offset}} = -200\text{G}$. The magnetic field is shown in Fig.(2.10). The slowing beam is red-detuned by $\approx -350\text{MHz}$ and does not interfere with the atoms in the MOT. The disadvantage of this setup comes with the zero-field region, here atoms can be optically pumped into the dark hyperfine ground state and need additional repumper light to stay in the cycling transition.

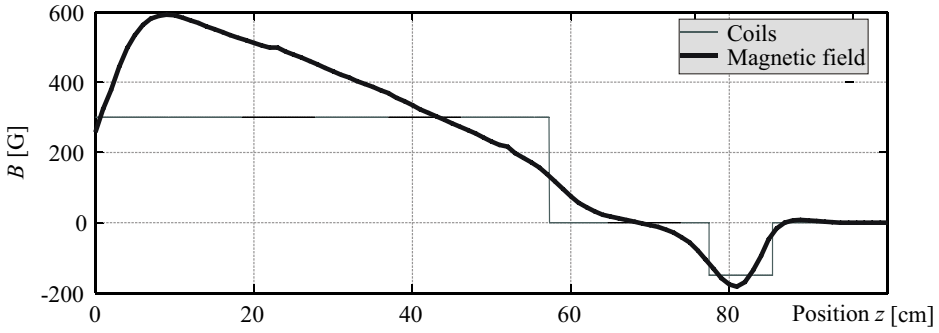

Figure 2.10: Inhomogeneous magnetic field of our Zeeman slower [26].

The Zeeman slower implemented in our experiment is optimized for sodium, as its capture velocity of 800m/s corresponds to the average velocity of hot sodium atoms. However, only a small fraction of the Maxwell-Boltzmann-distribution for lithium at 800K is below the capture velocity. On the other hand, due to the low mass of lithium, we get a higher maximum deceleration which allows for efficient slowing at lower intensity compared to sodium. Further details to our slower can be found in the diploma thesis of Jan Krieger [26].

Sodium MOT

In order to trap the slow atoms coming out of the Zeeman slower, three pairs of counterpropagating laser beams with the diameter of 25.4mm are crossed in the center of the glass cell. The intensity in each beam corresponds to the saturation parameter $s_0 \approx 1$. Magnetic coils in an anti-Helmholtz configuration create a quadrupole field with the zero point in the center of the laser beams. Repumper light is added via two extra beams with the same size as the MOT beams. The required laser light at a wavelength of 589nm is provided by a dye laser. The dye, Rhodamin 6-G, is pumped by a Radiant Dyes MonoDisk laser running at a wavelength of 515nm and delivering 2×6W of power. All required frequencies are generated using acousto-optical (AOM)

and electro-optical modulators (EOM). The principle of function of the dye laser as well as the laser system for the sodium MOT are treated in the diploma thesis of Stefan Weis [34].

Dark Spot In order to increase the density in the MOT, a so-called dark-spot technique is used [35]. In a usual, bright MOT the density is limited to $\approx 10^{11}$atoms/cm^3 due to the reabsorption of scattered light and a thus resulting repulsion between the atoms [36].[6] In order to further increase the density we want to suppress the scattering of the light in the center of the MOT. This is achieved by creating a region where repumping light is absent. Atoms entering this region are eventually pumped into the $F = 1$ ground state and become transparent for the MOT light. At the borders of this dark region, escaping atoms are repumped into $F = 2$ state and are driven back by light forces. The density in the dark region can thus be increased by a factor of 10! In our experiment the region without repumping light is realized by masking the center of the repumper beams with a dark spot, which results in two repumper tubes, and overlapping them in the center of the MOT.

Magnetic Trap and Evaporative Cooling

Placing an atom into a magnetic field shifts its levels according to the Zeeman effect, as discussed in paragraph(2.1.1). A Breit-Rabi diagram in Fig.(2.11) shows the different shifts of the magnetic sub-states. Interesting for us is the fact that there are states, that lower their energy for high fields and are therefore called high-field seekers, while low-field seeking states are those that lower their energy at low fields. Since a static maximum of the magnetic field in three dimensions cannot be created [37], we trap a low-field seeking state in a minimum of the magnetic field [38]. Besides, the anti-Helmholtz configuration of the MOT-coils already provides us with a quadrupole field with zero field in its center. Sodium BECs have been produced using either $F = 2, m_{\mathrm{F}} = 2$ or $F = 1, m_{\mathrm{F}} = -1$ state. We are going for the latter since the preparation of $F = 2, m_{\mathrm{F}} = 2$ is more demanding [39]. The transfer from the dark spot MOT into the magnetic trap is done by switching off the trapping light and rapidly ramping up the field gradient to compensate the light forces. The repumper light is switched off prior to the MOT light. This results in optical pumping of all atoms into the $F = 1$ state, its population is equally distributed among the three magnetic sub-states. Once the laser light is off, only atoms in $m_{\mathrm{F}} = -1$ state are trapped, while the others get lost. Therefore, a transfer efficiency of about 1/3 is achieved.

[6] Another density limitation is the two-body loss rate discussed in section (2.1.3).

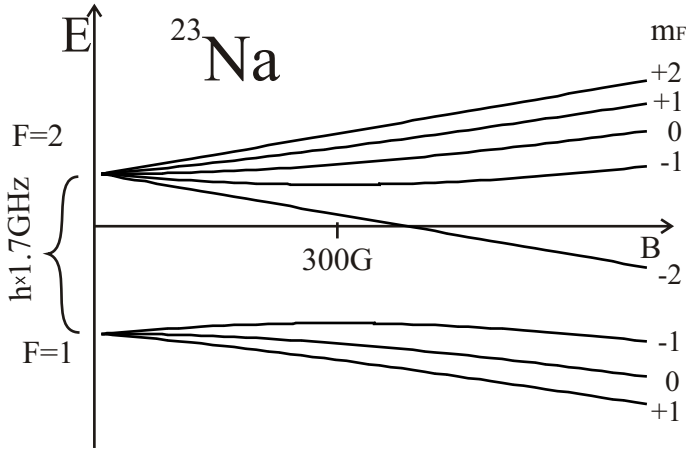

Figure 2.11: Breit-Rabi diagram for sodium shows the energy shifts of different states depending on the magnetic field. Low-field seeking states have a positive slope in the diagram.

Evaporative cooling The process of evaporative cooling can be described in following steps:

1. Remove the most energetic atoms from the sample.
2. Wait until the remaining atoms thermalise at a lower temperature.
3. Iterate the first steps until the desired temperature is reached.

This process can be also performed in a continuous way. Immediately, several questions arise:

1. How to selectively remove the hottest atoms?
2. How long do we have to wait for thermalisation?

To selectively remove the atoms with highest kinetic energy we make use of the existence of high-field seeking states. Atoms with high kinetic energy are more likely to reach high magnetic fields than the slow atoms. We drive a microwave transition to the untrapped $F = 2, m_{\mathrm{F}} = -2$ state with a detuning corresponding to the Zeeman shift at high magnetic field. Once an atom reaches a specified magnetic field, it is transfered into the high-field seeking state and immediately accelerated out of the trap[40]. The frequency of the microwave can be adjusted to remove atoms at lower fields as soon as the cloud is thermalised. Unfortunately, background pressure

limits the lifetime of atoms in the magnetic trap and does not allow for very long thermalisation times. As the process of thermalisation itself relies on elastic collisions between the atoms, the thermalisation rate depends on the collision rate and therefore on the density of atoms. In order to boost the collision rate, the magnetic trap is compressed by adiabatically raising the magnetic field gradient to 330G/cm in radial direction. However, one has to differentiate between elastic collisions leading to thermalisation and often called 'good' collisions and 'bad', inelastic collisions leading to heating and losses in the trap. An accurate analysis of the adiabatic compression as well as the evaporative cooling using microwave radiation used in our experiment is given in the thesis of Anton Piccardo-Selg [41].

One important feature of the quadrupole field is its zero crossing. For decreasing temperatures the atoms are more and more likely to be located close to the zero field. For $B = 0$, the m_{F} component of the angular momentum is not defined and an atom can be transfered into an untrapped state by a non-adiabatic spin-flip. In order that the spin of an atom follows the direction of the magnetic field, the Larmor frequency given by $\omega_L = \frac{|\mu B|}{\hbar}$ has to be larger than the rate of field's direction change seen by the atom. The region where the so-called Majorana loss can occur has a radius of [42]:

$$r_M \propto \sqrt{v\hbar/\mu B'} \tag{2.15}$$

with v being the velocity of the atom, and B' the gradient in the direction of its motion. In our case, for temperatures where Majorana losses become important r_M is in the order of few μm. To stop losses through this hole, we have to repel the atoms from that region using an optical plug.

Optical Plug To repel atoms from the hole, we introduce a repulsive potential by focusing a far blue-detuned laser into the zero field region[2].

The force producing this potential is called the dipole force and can be motivated using a dipole model of the atom. In this approach, the electron is bound to the atom via a damped spring and can be driven by an external electric field. As long as the induced dipole follows the driving field, it is attracted into the region of high amplitude of the external field. This corresponds to a red-detuned laser beam. For driving frequencies higher than the resonance frequency of the dipole, the electron cannot follow the field and the oscillation of the field is ahead by a phase of π. This means, that the dipole is anti-aligned with the electric field and it is repelled from the high intensity region. The dipole potential created by a far off-resonant

beam with intensity I and detuning δ is given by[43]:

$$U_D(r) = \frac{3\pi c^2}{2\omega_0^3}\frac{\Gamma}{\delta}I(r) = \frac{\hbar\Gamma^2}{8\delta}\frac{I(r)}{I_{\mathrm{S}}} \tag{2.16}$$

With a laser beam at a wavelength of 515nm and power of approximately 1W, focused to a waist of $w = 10\mu$m, we produce a 800μK high potential for sodium.[7] As soon as the focus of the beam hits the zero field, the Majorana losses are suppressed, which is confirmed by a longer lifetime of atoms in the MT compared to the situation without plug. For a description of finding of the zero field and a quantitative analysis of the plug refer to [44].

2.3 First signs of Bose-Einstein condensation

This section shows preliminary results of evaporative cooling of sodium atoms in the $F = 1, m_{\mathrm{F}} = -1$ state to 5μK and first signs of a Bose Einstein condensate (BEC) in our optically plugged magnetic trap.

2.3.1 Imaging

All information on the state of our atoms is obtained with absorption imaging. A short resonant light pulse is shone at the atoms. Due to absorption attenuated light is imaged on a CCD-camera. This absorption image is then used to reconstruct the density distribution of the atomic cloud. We use an imaging beam with an intensity far below the saturation intensity. This allows us to apply Lambert Beer's law for the reconstruction:

$$I(x,y) = I_0(x,y)e^{-\sigma\int n(x,y,z)dz} \tag{2.17}$$

where $n(x,y,z)$ is the number density of atoms and σ is the scattering cross section. Since we are interested in the density n, we first take a picture with atoms, this corresponds to $I(x,y)$, a second shot is taken under the same conditions, but without atoms, giving us $I_0(x,y)$. A third, background image is taken with all light off. At resonance and $s_0 \ll 1$, σ is given by [45]:

$$\sigma = \frac{\hbar\omega}{I_S}\frac{\Gamma}{2} \tag{2.18}$$

Solving Eq.(2.17) yields:

$$n'(x,y) = \int n(x,y,z)dz = \frac{1}{\sigma} ln\left(\frac{I_0(x,y)}{I(x,y)}\right) \tag{2.19}$$

[7] For lithium, the hight of the potential would be 391μK.

Actually, what we get is the the number density integrated along the beam path. Each pixel of the resulting picture corresponds to a column density. The total number of atoms is basically given by the sum of all pixels. Apart from the position and size of the cloud, one can also extract the momentum distribution for clouds undergoing free expansion [46].

2.3.2 Transition temperature

Two questions should be answered before the condensation. The first is: *When* do we expect something to happen? *When* means at 'which temperature'. We can estimate the transition temperature for our trap as follows: a quadrupole magnetic trap combined with an optical plug focused at the field zero creates a potential with two minima [41]. The bottom of each minimum can be approximated by an anisotropic harmonic potential. The transition temperature for a three-dimensional anisotropic harmonic potential is given by [47]:

$$T_C = \frac{\hbar\bar{\omega}}{k_B}\left(\frac{N}{1.202}\right)^{(1/3)} \tag{2.20}$$

with $\bar{\omega} = \sqrt[3]{\omega_1\omega_2\omega_3}$ as the geometric mean of the trap frequencies. In our case, $\bar{\omega} \approx 2\pi \times 1kHz$ due to the high gradient of the magnetic field. Plugging possible atom numbers into Eq.(2.20), we expect something to happen in the following temperature range:

- for $N = 10^6$ atoms: $Tc = 4.5\mu K$
- for $N = 10^5$ atoms: $Tc = 2\mu K$
- for $N = 10^4$ atoms: $Tc = 1\mu K$

These figures show that we are not very sensitive to the number of atoms.

Temperature measurement

We can measure the temperature of the atoms by suddenly switching off the trapping potential and observing the free expansion of the atoms. For a sufficiently long expansion time t_{TOF}, the shape of an expanding thermal cloud does no longer depend on the trapping potential and becomes a Gaussian with the width:

$$\sigma = \sqrt{\sigma_0^2 + \frac{k_B T t_{TOF}^2}{m}} \tag{2.21}$$

σ_0 being the width of the cloud for $t = 0$.

An independent estimate can be also obtained from the progress of evaporation. In a thermalized cloud the temperature is about 10 times lower than the trap depth [48].

2.3.3 Indication of condensation

The second question is: *What* do we expect to happen? There are several evidences for formation of a BEC. Major ones are the bimodal momentum distribution and the anisotropic expansion. For temperatures below T_C we expect the time-of-flight distributions to change from a single Gaussian to a bimodal distribution consisting of a broad thermal Gaussian cloud, and a narrow distribution corresponding to condensed atoms.[8] The anisotropic expansion of a BEC is related to the interaction of the atoms, therefore the direction of stronger confinement in the trap is the one in which the cloud is expanding faster than in the other.

Fig.(2.12) shows a series of expansion images after a time-of-flight of 3ms at different moments of evaporation. The profile of the first image is very well approximated by a Gaussian. Its temperature can be estimated to 7μK by using the width of the cloud, the number of atoms is about $8 \cdot 10^5$. The trap depth is about 50μK. Further evaporation reduces the number of atoms to $4 \cdot 10^5$ and the profile changes qualitatively since it cannot be fitted by a single Gaussian anymore. This bimodal distribution is even more obvious in the last shot. The profile is a sum of a Gaussian and a narrow parabola corresponding to atoms in the condensate. The temperature of the thermal cloud is about 2μK in a 15μK deep trap.

The emergence of the bimodal distribution is one of the evidences of Bose-Einstein-Condensation. Another, less strong sign is the change of aspect ratio of the cloud, which can be seen in Fig. (2.12). While the thermal cloud in a) is perfectly round, the atoms on the last image have an elliptical distribution. The observed anisotropic expansion is in qualitative agreement with the oscillation frequencies of our potential.[9]

The high transition temperature and the early appearance of anisotropic expansion can be both attributed to relatively high confinement in our magnetic trap.

[8] Atoms in the ground state have negligible kinetic energy.[17]

[9] In vertical direction $f_v = 1$kHz, in horizontal direction $f_h = 1.7$kHz [41]

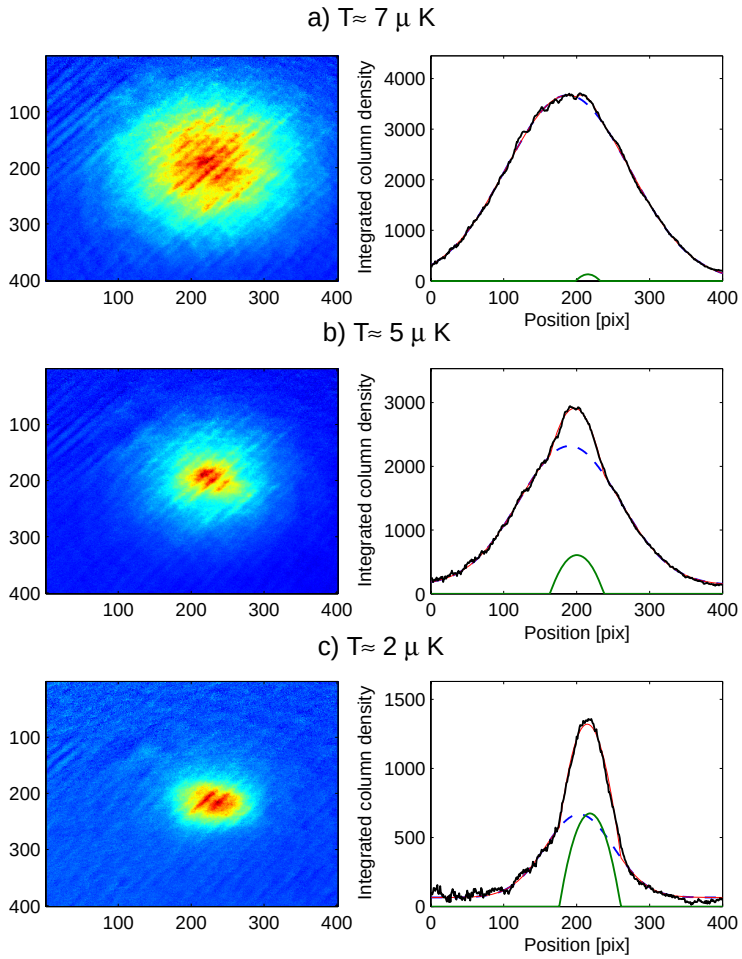

Figure 2.12: Emergence of a bimodal distribution. All images are taken after a time-of-flight of 3ms. The corresponding profiles are created by integrating along the horizontal direction. $8 \cdot 10^5$ atoms expand classically in Fig. a).The Gaussian fit is indicated by the dashed lines. Figures b) and c) show an emerging parabolic distribution inside of the thermal cloud for decreasing temperatures. This can be attributed to the condensation of sodium. The fit of the combined model is indicated by a red line. The shape of the cloud changes from a round to an elongated one.

2.3.4 Conclusion

Although we can reach degeneracy of sodium gas, the system has to be optimized for a higher number of atoms for two reasons. Sympathetic cooling

of lithium will cost more sodium atoms during the evaporation to reach the same temperature. The second reason is that we want to cool as far as possible into degeneracy to have no thermal effects in the future polaron experiments.The implementation of cooling and adding of lithium-6 atoms is the topic of the next chapter.

Chapter 3

Lithium, the impurity

"das Salz in der Suppe"[1]

Fermionic lithium-6 atoms will play the role of impurities in the Bose-Einstein condensate (BEC). Compared to sodium, much less lithium is needed. Nevertheless, we will see that transferring lithium from one trap to another is a lossy business [32], the goal is therefore to start with 10^7 to 10^8 atoms in the MOT and make sure, that at the end of the day, at least 10^4 lithium impurities are left within the condensate.

In this chapter the lithium part of the experiment is described. The laser cooling of lithium begins with setting up of the necessary spectroscopy. The locking scheme is briefly depicted. The lithium setup consisting of the laser system and the lithium upgrade to the existing sodium setup is described. Magneto optical trapping of lithium will be characterized and optimized for both, high lithium number and compatibility to the sodium parameters. First results of compression and loading into the magnetic trap will be given at the end of this chapter.

3.1 Laser cooling of Lithium

The scheme for laser cooling and trapping of *sodium* works basically as described in section (2.1). Due to finite energy splitting of hyperfine states, transition to a 'wrong' excited state is allowed, deexcitation into the dark ground state is not forbidden anymore. Merely a weak repumper beam is required in order to pump atoms from the dark state back to the cycling

[1]The literal translation is "the salt in the soup", an idiomatic expression for "has that little extra something", also means the most important but not very obvious ingredient.

transition (see section (2.1.3)). The situation is different for lithium: The hyperfine structure of the excited state is not resolved since the energy splitting is smaller than the natural transition width of $\approx 2\pi \times 6MHz$ (see Fig.(3.1)) and we get an effective three-level scheme. The consequence is that MOT and repumper beams should have about the same scattering rates [49]. Otherwise one of the ground states would be populated stronger than the other, leading to inefficient cooling and trapping.

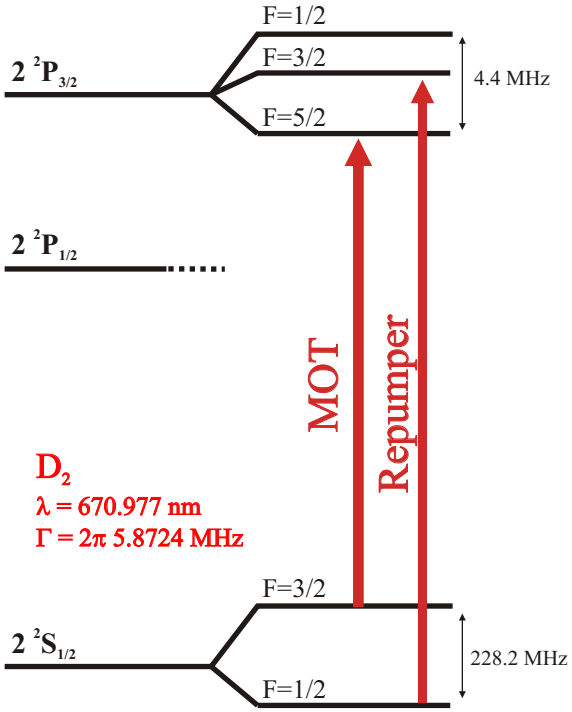

Figure 3.1: ^{6}Li level scheme. Transitions of the D1 line have been omitted.

Tapered amplifier laser system

The laser light for lithium MOT is provided by a tapered amplifier system (TA100). It is a grating stabilized diode laser [50], amplified by a tapered semiconductor amplifier, delivering about 390mW of single frequency light. The frequency can be tuned around the lithium D2 line using the piezo actuator mounted to the grating. The beam power is split over MOT, repumper and slower beams in a ratio of about 2:1:1.

3.2 Spectroscopy Locking

As shown in section (2.1), the atoms are sensitive to differences of detuning in the order of $\Gamma/2$. To be able to create and manipulate a MOT, the frequency of the laser must be controlled with a precision better than $\Gamma/2$. Fortunately, the line width of our laser is below 100kHz, given by the external resonator. The frequency of our diode laser depends on the current, the grating angle and the temperature of the diode. All of these parameters are electronically kept constant, resulting in a stable output frequency. Nevertheless, drifts over long periods are unavoidable since no absolute reference is available. To establish an absolute frequency reference, a spectroscopy has been set up. The spectroscopy cell used in the experiment is described in the following section. The frequency-modulated spectroscopy technique is used for locking of the laser. The progress of putting the spectroscopy cell for lithium into operation, as well as the generation of the locking signal are given in detail in appendix (A).

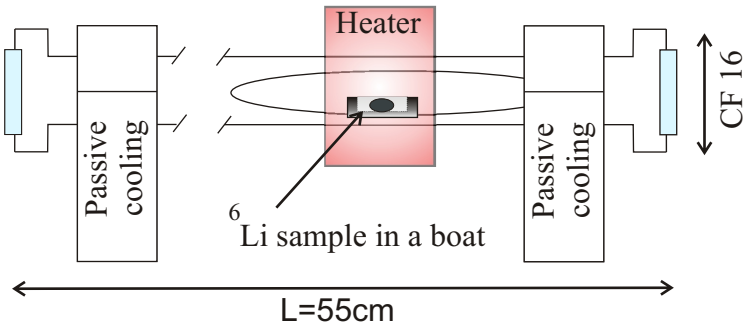

Figure 3.2: The spectroscopy cell. The heater runs at 330°C producing enough lithium vapor for absorption spectroscopy. Because of the low heat conduction properties of steel and the two massive blocks of aluminum holding the steel tube and acting as heat dissipators, the windows are at room-temperature. The crucible (boat) containing the lithium sample shall localize lithium and facilitate refilling of the cell.

3.2.1 Spectroscopy cell

A reasonable absorption signal of a few percent is obtained at a partial vapor pressure of about 10^{-5}mbar. Due to the low vapor pressure of lithium compared to other alkali metals, a lithium simple has to be heated above 330°C. Usually, the vapor is prepared in a heated cell with glass windows for optical

access. However, glass undergoes a chemical reaction with hot lithium gas and therefore becomes opaque. A heat pipe, built to circumvent this problem, is illustrated in Fig.(3.2) and Fig.(A.8). A steel crucible containing a piece of lithium lies in the center of a 55cm long steel tube which is heated only locally. The outer ends are cooled passively with large aluminum blocks. The length of the tube and the low heat conductance of steel contribute to the fact that the glass viewports remain at room temperature and are not in direct contact with hot lithium gas. Lithium atoms get stuck when hitting the cold wall and do not reach the viewports. Prior to filling, the cell has been baked out at 230°C for 24 hours. The first signal of absorption was detected after operating the cell at 500°C for a few minutes. To prevent coating of the windows, 0.1mbar of argon was introduced into the cell after putting it into operation. Single pass transmission of 671nm light through the heat pipe with new windows is 52%. Normal operation temperature is 330°C.

3.2.2 Doppler-free, frequency-modulated spectroscopy

The absorption spectrum of a thermal gas, especially at 330°C, is broadened by the Doppler-effect. To get rid of the Doppler-broadening of the absorption signal we use a combination of a pump and a probe beam, as it is explained in appendix (A). The laser is locked to the frequency of the largest feature of the absorption, being the crossover between the two hyperfine lines, shown in Fig.(3.3). The derivative of the absorption signal is used as feed-back for the PI-controller to stabilize the frequency of the laser. In order to obtain the derivative, the frequency of the beam used for spectroscopy is modulated and the absorption signal is fed into a lock-in amplifier, see section (A.4). The lock-in amplifier acting as a narrow band-pass filter, amplifies the signal at the modulation frequency and suppresses the noise on all other frequencies. The resulting error-signal is presented in Fig.(3.3).

3.3 Laser setup

The laser system for lithium consists of the spectroscopy and the optics for the generation of necessary frequencies. The generation of frequencies is explained below. The laser light is subsequently transported via optical fibers to the experimental table, where additional optics are installed to allow for simultaneous operation of the sodium and lithium MOTs, this upgrade is covered thereafter.

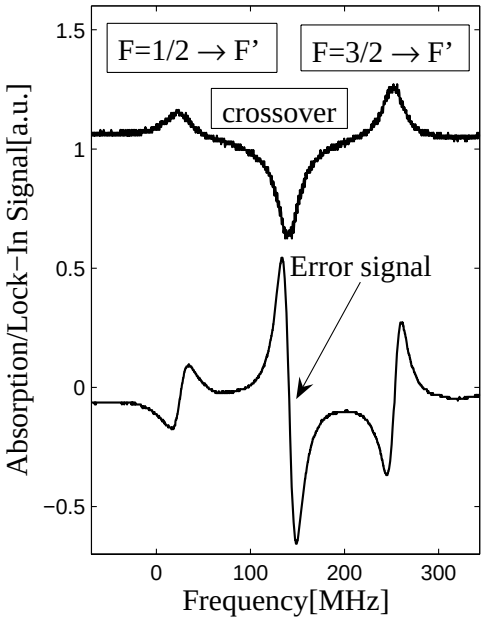

Figure 3.3: Pure photodiode signal with transition lines and their crossover, below is the output signal of the lock-in amplifier. The largest slope is used for locking of the laser.

3.3.1 Frequencies and Optics

The frequency-modulation of the laser described in the last section is done with an AOM running at $f_{\text{spectr}} = 150\text{MHz}$, and since we double-pass the first diffracted order before doing spectroscopy, the overall detuning of the laser is $-2 \times f_{\text{spectr}} = -300\text{MHz}$ relative to the crossover. With a hyperfine splitting of 228MHz, transitions from $F = 3/2$ and $F = 1/2$ are respectively -114MHz and $+114\text{MHz}$ away from the crossover. We shift the frequency of the laser with additional AOMs to get all required frequencies. Table (3.1) summarizes necessary laser beams and the corresponding frequencies.

MOT and Repumper

For the operation of a lithium MOT, two laser frequencies are required, one frequency for the transition from $F = 3/2$ to $F' = 1/2, 3/2, 5/2$, that is used as the cooling transition and is denoted by *MOT*-frequency. Excited atoms in $F' = 1/2, 3/2$ are allowed to decay into the $F = 1/2$ ground state, therefore a second, so-called *repumper*-frequency, that drives the transition from $F = 1/2$ to $F' = 1/2, 3/2$ is necessary.

Purpose	*Transition*	*Detuning rel. to laser*	*Detuning rel. to transition*
Locking	Crossover	300MHz	0MHz
MOT	$F = 3/2 \rightarrow F'$	160MHz	-25MHz
Repumper	$F = 1/2 \rightarrow F'$	400MHz	-15MHz
Slower	$F = 3/2 \rightarrow F'$	-164MHz	-350MHz
Slower Repumper	$F = 1/2 \rightarrow F'$	64MHz	-350MHz
Imaging	$F = 3/2 \rightarrow F'$	184MHz	0MHz

Table 3.1: Preliminary frequencies. To optimize the MOT performance, detuning of beams will be modified.

Zeeman Slower

Same as for the sodium MOT, the lithium MOT is loaded from an atomic beam coming out of the Zeeman slower. The slowing laser beam has to be detuned by -350MHz relative to the MOT transition in order to deliver atoms cold enough to be captured by the MOT. This frequency is basically predefined by the settings of the slower optimized for the sodium MOT. For the slower beam, a repumper component (see section (2.2)) is generated with an extra single-pass AOM at 228MHz.

Imaging

Finally, for the purpose of taking data, an independent beam with resonant light is needed. A provisional imaging is set up using a double-pass AOM. This set-up can only be used for zero-field imaging, since the bandwidth of the AOM is limited to 20MHz. A superior system, using offset locking allowing for eventual imaging at high magnetic fields, has been integrated by Bernhard Huber [51]. The offset imaging consists of an additional diode laser. A fraction of its output is overlapped with light from the main laser to create a beating signal. This beating signal allows for locking of the diode laser relative to the main laser at any frequency difference up to 2GHz.

Layout

In order to shift the frequency, standard AOMs in doube-pass configuration have been used. The overall efficiency of double-passed AOMs of about 70% (at center frequency) could be achieved using by cylindric lenses to match the beam shape to the active aperture of the AOMs. The layout of the laser system for lithium illustrated in Fig.(3.4), is similar to sodium setup

[34]. It consists of a main 'artery' and polarizing beam-splitter cubes, that distribute power among MOT-, repumper- and slower-beams. Single-mode fibers are used to transport the light to the experimental table, as well as spatial filters. MOT and repumper beams are coupled independently into two different inputs of a 2-to-6 fiber splitter, so no overlapping of the beams is needed. Another advantage of using different ports is that polarization of both beams can also be chosen independently.

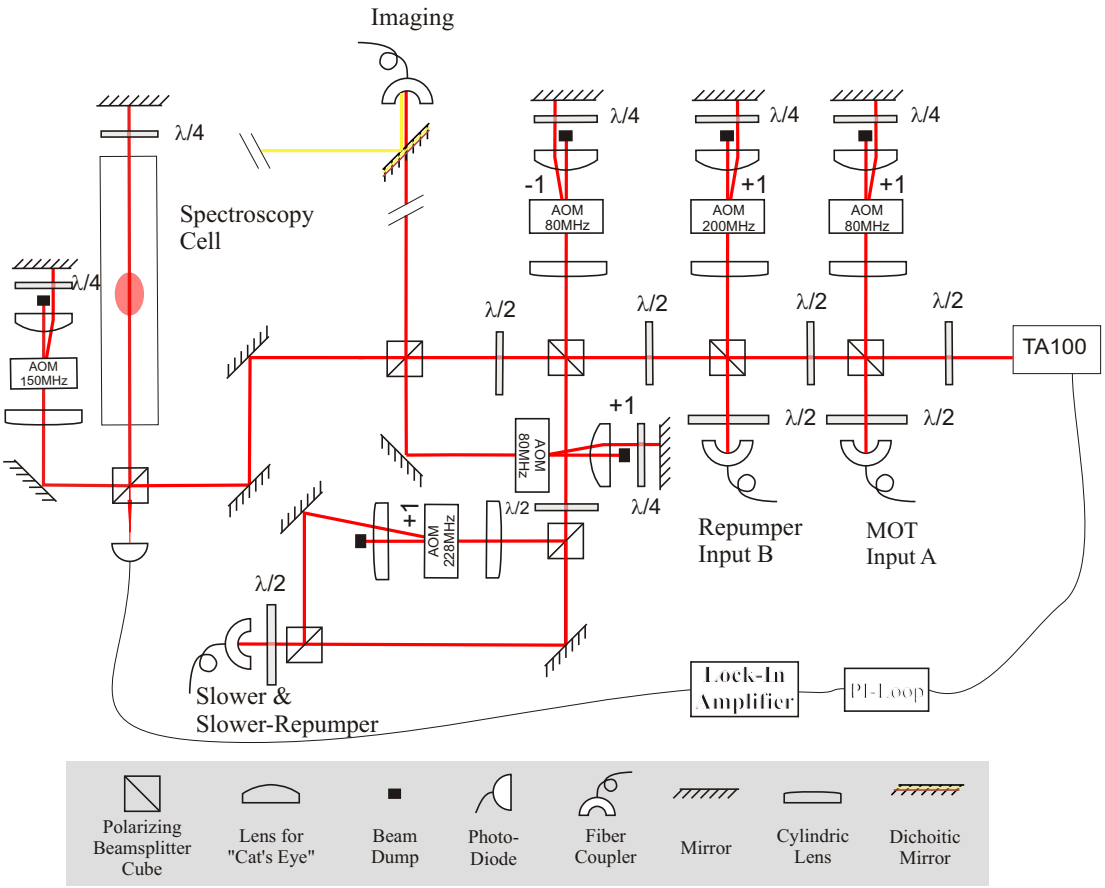

Figure 3.4: Lithium laser system. The tapered amplifier delivers 360 to 390mW. About 160mW are split off at the first cube for MOT light. Repumper and slower light get each 100mW of power. The remaining few mW's are used for imaging and spectroscopy.

3.3.2 Lithium Upgrade

Setting up the laser system for lithium is done independently of progress in the sodium part. As soon as all fibers are coupled, the configuration of laser beams for sodium on the experimental table has to be adopted. The concerned sections are: MOT beams, Zeeman slower and imaging light. The key element for the upgrade are dichroic mirrors.

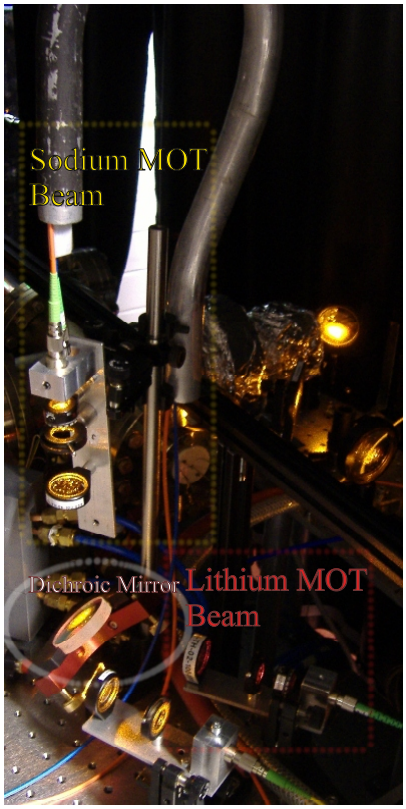

Figure 3.5: Overlap of the MOT-beams. Assemblies for the MOT beams are described in Ref.[34]. The sodium MOT beam is mounted vertically. A two-inch large dichroic mirror, shown in the lower left-hand corner, is used to overlap the two beams. The aluminum 'hook' serves as a protection for the sodium MOT fiber.

MOT Beams

The main difficulty is to add six additional one inch large beams directed to the center of the glass cell, without reducing optical access. The most economic way (in the sense of optical access) is to overlap the additional

beams with the existing ones, see Fig.(3.5). Mirrors, highly reflective (> 99%) for sodium light and highly transmitting (85%) for 671nm light, are used to overlap the MOT beams. We have chosen HR589HT671 coating to keep the intensity of sodium light, since large sodium atom numbers are essential for successful evaporative and sympathetic cooling.

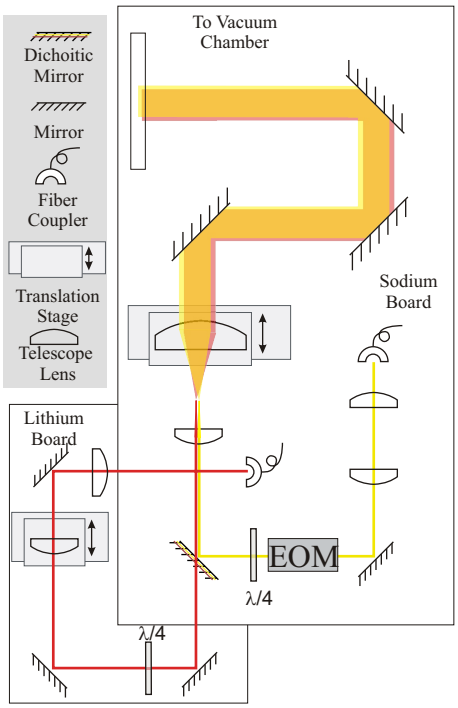

Figure 3.6: Slower upgrade. The translation stage in the lower left hand part of the picture can be used to change the width of the slowing beam for lithium.

Slower Beams

While other possibilities for the MOT beams are imaginable, there is no way around overlapping the slowing beams. The upgrade for the slower is illustrated in Fig. (3.6). For sodium light, only one mirror has to be replaced by a dichroic one, without any changes to the trajectory of the beam. The slowing beam for lithium is set up on an additional breadboard. Main feature of this setup is an extra telescope, that can be used to independently adjust the final width of the lithium slowing beam.

Imaging Beams

The imaging beams for sodium and lithium are overlapped and coupled into the same optical fiber. This way sodium imaging system including the camera can be used for lithium, too[44]. Except for overlapping of the beams, no additional optics are required.

3.4 Lithium MOT

The performance of the lithium MOT, that is basically the loading rate, achievable atom numbers and temperatures, is presented in the current section.

Two major goals are pursued. The first objective is to understand the interaction of available parameters and their influence on the figures of merit. The main goal, however, is to optimize the lithium MOT with respect to sodium. For the polaron experiment, where lithium plays the role of impurities, the density of lithium should be much smaller than the density of the sodium condensate. Therefore, as long as we can measure the motion of lithium within the condensate, the goal is met. Additional lithium would only 'cost' more sodium as refrigerant.

3.4.1 Consideration on Parameters

What are the knobs we can turn to optimize the MOT? In the following, the available parameters and their expected influence are outlined.

Detuning

A short reminder of the results from the introduction to laser cooling: the capture range and capture velocity of a MOT both increase with larger detuning. At the same time, the scattering rate decreases. Starting from small detuning, we expect the performance to improve with increasing detuning, until the scattering force is too weak to trap the atoms. We will investigate this dependence.

Laser power and intensity

The tapered amplifier, delivers up to 390mW. Considering the efficiency of 70% of double-pass AOMs and fiber-coupling efficiency of 45%, only about 120 mW reach the experimental table. Taking the dichroic mirrors (with a transmittion of 85%) into account reduces the total power to 100mW. The

distribution between MOT, repumper and slower beams has to be done very carefully. As a rule of thumb and considering the dependence of the scattering rate on intensity, each MOT beam (out of six) should have intensity in the order of saturation intensity $I = I_S = 2.54\text{mW/cm}^2$. The intensity of the repumper component in the beams should be of the same order of magitude as the cooling component, though transition strengths (shown in appendix (B.1) indicate that actually less intensity in the repumper component may suffice. The intensity of the slowing beam must be high enough to ensure that atoms do not escape deceleration due to imperfections of the magnetic field.

Magnetic Fields

The lithium MOT obviously shares the same magnetic field gradient with sodium MOT. The same is true for the magnetic field of the Zeeman slower. Therefore, the MOT gradient is the main constraint for lithium MOT, whereas, magnetic fields optimized for sodium should be only more conservative for lithium [26] .

3.4.2 Taking Data

Absorption imaging is one way to analyze the MOT. The MOT can be also monitored by measuring the fluorescence of the atoms. Fluorescence signal gives an estimate to the number of atoms and allows to observe the dynamics of loading and decaying of a MOT. Since both techniques will be applied, a short introduction is given in the following section.

Fluorescence Measurements

In a MOT, trapped atoms are constantly absorbing and reemitting light. The power of the fluorescence is therefore directly proportional to the number of trapped atoms.[2] Since the reemission is isotropic, the intensity of fluorescence into a solid angle Ω subtended by a lens is still proportional to the atom number. We measure the fluorescence with a photodiode (PD). In order to extract the absolute number of atoms out of the PD voltage, one would have to solve the following equation for N:

$$P_{\text{atoms}} = N\hbar\omega_0\gamma_{\text{scatter}}(\delta, s_0)\Omega = P_{\text{PD}} = \frac{U_{\text{PD}}}{R_{\text{Load}}\epsilon(671\text{nm})} \tag{3.1}$$

[2]This is true for low densities, at higher densities one systematically underestimates the number of atoms due to radiation trapping.

with $\epsilon(671\text{nm}) = 0.44\text{A/W}$ being the responsivity of the photodiode, and $R_{\text{Load}} = 1\text{M}\Omega$ being the resistance of the oscilloscope. For every uncoated glass surface traversed by the fluorescence light, an additional factor of 0.96 has to be taken in account. Although, in everyday practice of aligning the beams and optimizing the slower, one is only interested in relative changes. The main advantages of fluorescence are its simple setup and the 'live' character.

Absorption Imaging

Absorption imaging is somewhat complementary to detection of fluorescence via a PD. Compared to the live response of a PD-signal, absorption imaging is rather slow: each shot takes in the order of tens of seconds, since a new sample has to be loaded into the trap. On the other hand, the procedure of imaging is automated and delivers spatial distribution of the atomic cloud and absolute atom numbers. A brief introduction to the theory of imaging is given in section (2.3.1).

The exposure time for lithium is only 20μs. Due to the low mass, illuminating lithium atoms over longer periods would accelerate the cloud and eventually disturb the picture by bringing the atoms out of resonance.

3.4.3 Optimizing Zeeman Slower

To slow as many lithium atoms as possible, the diameter d_S of the slowing beam should be chosen preferably as large as the inner diameter of the slower tube. On the other side, the deceleration $a = F_S/m = \hbar k\gamma/m$ depends on the intensity (which goes with $\propto 1/d_S^2$) and varies proportionally to intensity for values in the order of $I_{\text{S}} = 2.54\text{mW/cm}^2$. In fact, with a deceleration below a critical value, the slower should not work at all, since the resonance condition

$$\delta_0 + \delta_{\text{Doppler}} + \delta_{\text{Zeeman}} = 0 \tag{3.2}$$

cannot be fulfilled for the complete length of the slower. For high intensity, the deceleration saturates due to the maximum scattering rate of $\Gamma/2$. We would therefore expect the loading rate to saturate for high intensity as well.

The four datasets shown in Fig.(3.7) represent different settings for the distribution of the available laser power. The portion of laser power for the slower beam is increased by diverting it from the MOT and repumper beams. For each power setting, the intensity is changed via the diffraction efficiency of the slower AOM, while the diameter of the slower beam is constant for all measurements. The MOT loads for one second, a photodiode records

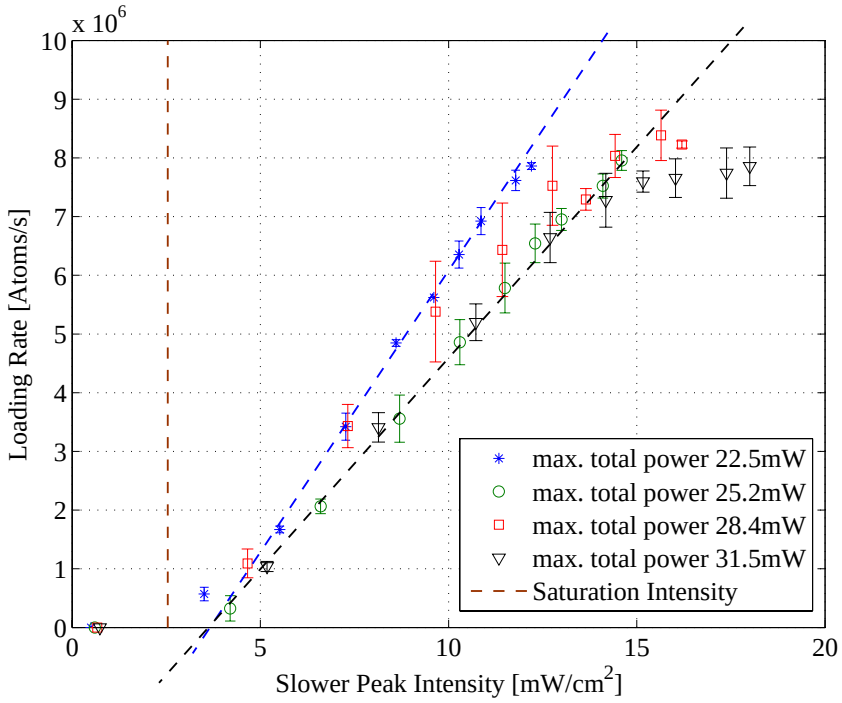

Figure 3.7: Power balancing between the slower and the MOT/repumper beams. The loading rates versus the intensity of the slower beam for four different settings is shown. The saturation intensity $I_S = 2.54$mW is denoted by the vertical dashed line. The loading rate grows linearly with the intensity for values between 5mW and 12mW, which is indicated by the dashed lines.

the fluorescence, which is then converted into a loading rate, as described in paragraph (3.4.2).

We can identify a linear dependence of the loading rate on the intensity for all settings in the range between 5mW and 12mW. Extrapolation of the linear part indicated by the dashed lines, does not go through the origin, but hits the zero line for a peak intensity around $3 - 4$mW. This value could correspond to a fulfilled resonance condition. For intensity below this value, even the smallest imperfection of the slower field, allows the atoms to leave the slowing process.

In the linear part of the curves, the wings of the Gaussian slower beam continuously cross the threshold intensity, that is necessary to slow an atom all the way. By that, the effective slowing area of the beam is extended with increasing intensity.

For intensity above 15mW the loading rate does no longer increase pro-

portionally to the intensity, as can be seen for data points denoted by the black triangles.[3] We also see that missing power in MOT/repumper beams leads to overall lower loading rates, when comparing the different settings at the same intensity.

Fig. (3.7) shows that that the loading rate is limited to 8×10^6atoms/s. The dependence of the loading rate on the beam diameter has not been checked systematically. A larger beam at the same intensity would certainly increase the loading rate, but requires additional power. Finally, it would be interesting to see what happens in the region around the saturation intensity and whether a real threshold intensity can be determined.

3.4.4 The Role of Detuning

The frequency-shift of the spectroscopy-AOM can be used to change the detuning of all beams at the same time.

The advantage compared to shifting each AOM individually, is that the diffraction efficiency of each AOM does not change, which is important when the output intensity has to be constant. The detuning δ_{Slower} of the slower beam directly enters in the final velocity of the atoms, resulting from the resonance condition Eq.(2.3):

$$v_{\text{end}} = \frac{\delta_{\text{Slower}} - \Delta\mu B_{\text{end}}/\hbar}{k} \tag{3.3}$$

To keep v_{end} constant, the magnetic field of slower can be adjusted to compensate for the change of detuning.

Atom Number and Temperature

The temperature can be determined by measuring the spatial extension of the cloud. We turn off the laser light and magnetic field gradient and let the atoms expand for a time of flight $t = 0.2 - 2$ms. The width of the cloud can be determined from the absorption pictures taken after a certain time of flight [46]. A series of measured widths is fitted to the model:

$$\sigma(t) = \sqrt{a + bt_{TOF}^2} \tag{3.4}$$

The fit parameter $b = \frac{k_B T}{m}$ yields the temperature of the cloud in the corresponding direction. Results are shown in Fig. (3.8,b). The temperature

[3] We expect, however, that with additional intensity the flux of cold atoms should always increase, at least, due to power broadening and the resulting higher capture velocity of the Zeeman slower.

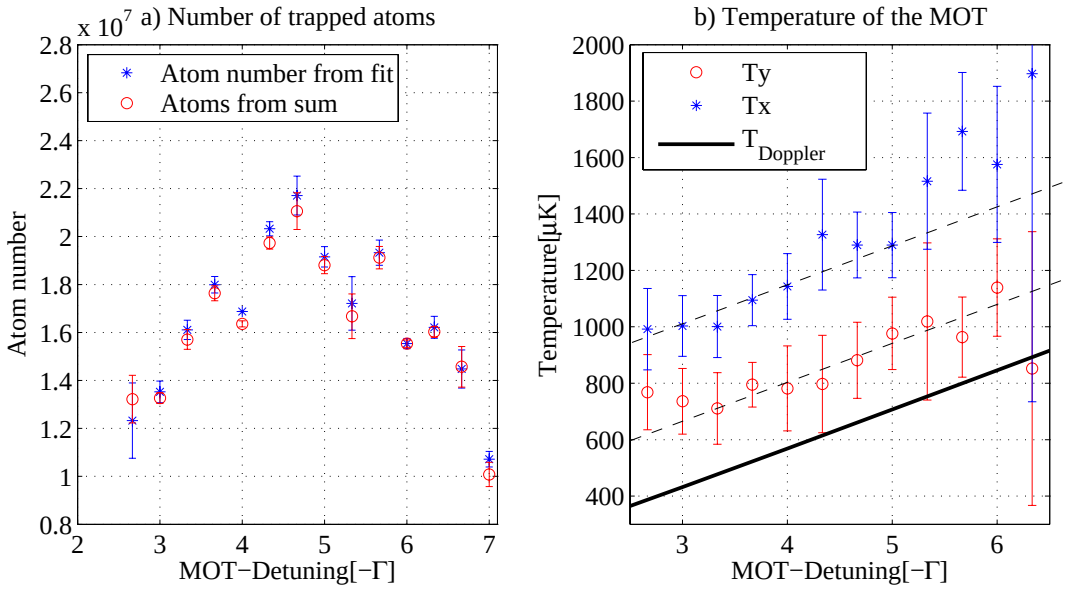

Figure 3.8: Number of atoms is calculated by summing over all pixels in the region of interest(o) or is obtained from the fit to profiles of the cloud(*). The fact that both calculations coincide, indicates that the density distribution is well described by a Gaussian. The plain line in Fig. b) corresponds the expected Doppler temperature given by Eq.(3.5), the dashed lines indicate the slope of the Doppler temperature and are shifted to fit the measured data. For each detuning, the MOT is imaged three times, the error bars display the standard deviation of the measurements. Error bars of temperature measurements show the 95% confidence bounds of the fitting routine.

curve is in qualitative agreement with the Doppler theory [23]:

$$T(\delta_0) = \frac{\hbar\Gamma}{4k_B}\frac{(2\delta_0/\Gamma)^2+1}{|2\delta_0/\Gamma)|} \tag{3.5}$$

As shown in Fig.(3.8,b), we have different temperatures depending on the direction of the expansion. For both directions, the temperature rises linearly with detuning and has the same slope (within the measurements accuracy) as the theoretical curve(solid line). The absolute values, however, have a positive offset of about 250μK for $T_{\rm y}$ and 500μK for $T_{\rm x}$. The temperature as a function of field gradient has not been investigated, nevertheless the data in Fig.(3.8,b) suggests that a lower temperature in y-direction may be related to the double gradient.

The number of atoms peaks for a MOT detuning of -4.5Γ. The increase of atoms for detuning $-3\Gamma \rightarrow -5\Gamma$ is what we expect for larger capture

ranges and velocities. The subsequent drop of atom number, however, can not be explained by simple arguments. One possible explanation is the scattering rate decreases with increasing detuning, so possibly, the intensity in the MOT beams is too low to efficiently load atoms from the atomic beam. If we are limited by intensity for large detuning, further reducing of the intensity must lead to a dramatic drop of atom numbers. It turned out however, that we could reduce the intensity by 10% without change in atom number. Another possible reason for the decreasing atom number may be a loss channel appearing for high detuning. To rule out this possibility lifetime measurements have been performed.

Lifetime and Density

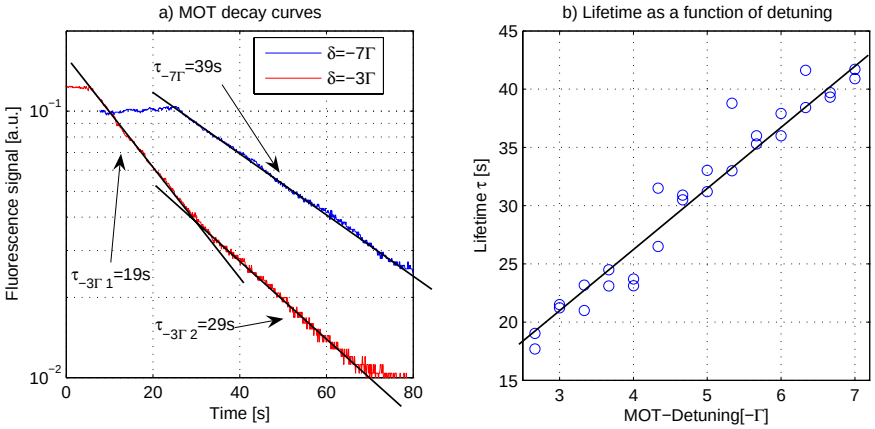

Figure 3.9: As an example, two decay curves are shown in a). The lifetime is characterized by the slope of the curve in the logarithmic plot. It corresponds to the decay constant τ for an exponential decay. For each detuning two decay curves are recorded. As in case of -3Γ in a), two different slopes can be drawn. In such cases, only the steeper ones have been taken into account for figure b).

The lifetime of the MOT is determined by recording MOT fluorescence after blocking the atomic beam and turning off the slowing beam. This is done for each detuning under the same conditions as for the data in Fig.(3.8). In Fig. (3.9,b) the lifetime as a function of the laser detuning is shown. No additional losses for large detuning can be identified. In contrary, the lifetime increases with the detuning. For MOT detuning below -5Γ, two different slopes can be distinguished. In Fig.(3.9,a) two extreme examples are shown: the decay curve for a detuning of -7Γ is clearly exponential with a lifetime

$\tau_{-7\Gamma} = 39$s, the other curve can be seen as composed of two exponential decays with $\tau_{-3\Gamma 1} = 19$s and $\tau_{-3\Gamma 2} = 29$s as lifetimes. An increasing lifetime is qualitatively in agreement with two-body loss model, even if the lifetime measurement does not explain the bad loading rate for large detuning. Main contributions to two-body losses are the radiative escape and state changing collisions, both depend on the population in the excited state, which is proportional to the scattering rate. At the same time, the two-body loss rate also depends on the density.

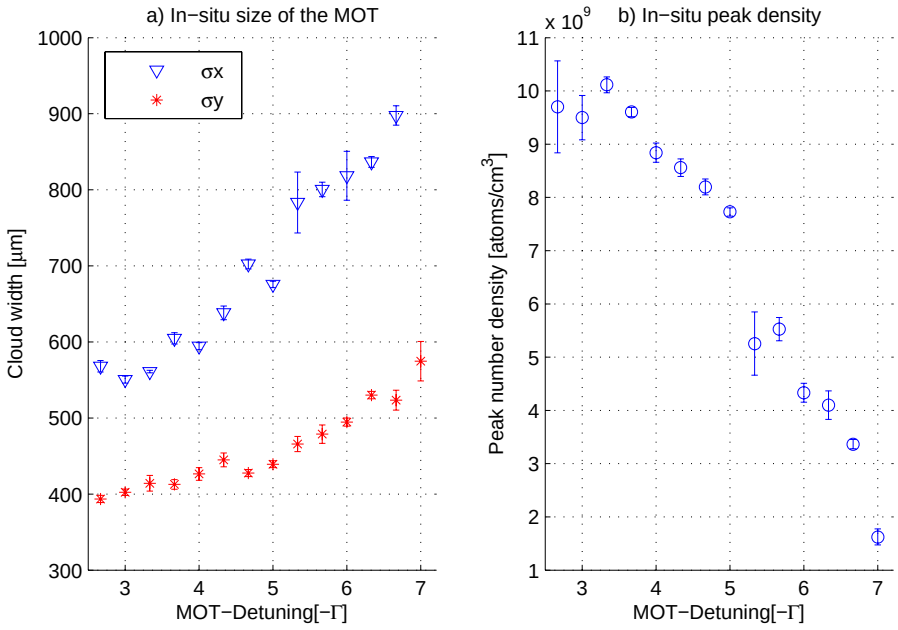

Figure 3.10: Size of the atomic cloud is given by the width of the Gaussian fit to the absorption image. Error bars indicate the standard deviation of three measurements.

The peak density as a function of the MOT detuning in Fig. (3.10,b) has been determined using absorption images. Despite the increasing atom numbers for detuning -3Γ to -5Γ (see Fig.(3.8)) the peak density decreases. This is related to the simultaneous increase of the volume of the cloud, as shown in Fig. (3.10,a). Returning to the issue with the lifetime, the question arises whether one could separate one- and two body losses. We would expect one-body losses to be independent of detuning. The contribution of two-body losses would decrease due to a lower scattering rate and also due to a decreasing density . Using a modified fitting model for the decay curve of

the MOT, including the two-body losses, however did *not* prove successful.

$$N(t) = \frac{N_0 e^{-t/\tau}}{1 + N_0 \tau \beta (1 - e^{-t/\tau})} \tag{3.6}$$

Two-body loss coefficients β as well as lifetimes τ resulting from fitting had a rather random character. Two possible reasons for that can be given. Slow drifts of polarization in MOT beams on a timescale of few seconds lead to a fluctuating fluorescence signal, altering the decay curve and making a good fit more difficult. This idea is supported by the fact that two decay curves taken at same conditions give very different fit results when using the two-body model. A rather speculative way to see the data is to suppose that there might be a process, which we have not considered yet, that kicks out single atoms out of the MOT and its rate $1/\tau(\delta)$ depends on detuning. This would explain the lifetime as a function of detuning as shown in Fig.(3.9,b).

In conclusion, the detuning of the laser beams has been scanned over a wide range and properties of the MOT were analyzed. We get the coldest MOTs for the smallest detuning of -3Γ, we obtain the longest lifetimes for the largest detuning of -7Γ, and to trap highest number of atoms the detuning has to be -5Γ, so which way to go? We will take the path of the largest MOT. As soon as lithum and sodium are transfered into the magnetic trap, lithium (literaly speaking, a drop in the bucket) will adopt the temperature of sodium, which presents a huge heat capacity due to higher mass of sodium atoms as well as the larger atom number in the sodium MOT.

3.4.5 Magnetic Field Gradient

The magnitude of the magnetic field gradient so far has been kept constant at 16.5G/cm in axial direction, being optimized for sodium MOT. How does the lithium MOT behave for different magnetic field gradients?

It turns out that at $B = 6.6$G/cm in axial direction the lithium MOT becomes very voluminous and unstable for a detuning $\delta_{MOT} \leq -5\Gamma$. In Fig. (3.11,a) atom numbers as a function of the MOT detuning are compared for two different gradients. At a critical detuning δ_C the MOT suddenly disappears at low field gradient. This critical detuning as a function of the magnetic field gradient is shown in Fig.(3.11,b). The reason for the observed instability may be the finite beam diameter. The force field (for an atom at $v = 0$) resulting from overlapping the optical molasses with a quadrupole field is illustrated in Fig.(3.12,a). By increasing the detuning, the ring of maximum force enclosing the center is shifted outwards. Due to the finite beam size, the force along the diagonals vanishes for large detunings and

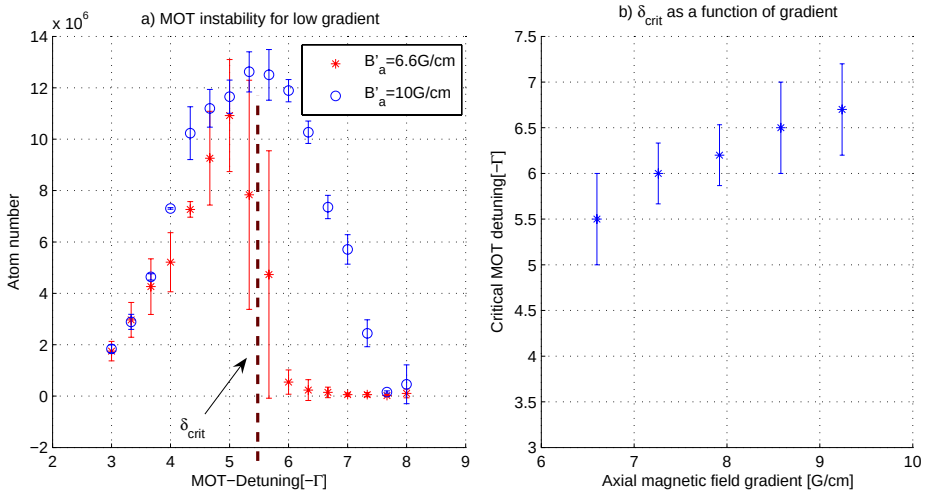

Figure 3.11: The detuning in a) is scanned using the AOM frequency of the MOT-component, the resonance-like envelope originates from the diffraction efficiency of the AOM. The error bars indicate the deviation of three measurements. For a 'critical' detuning indicated by the dashed line, the atom number of the MOT fluctuates, which can be seen in the very large error bars around the dashed line. This detuning is plotted for different magnetic field gradients in b), the error bars correspond to the width of the slope around the critical value of detuning.

atoms may escape from the trap. Increasing the gradient closes the holes along the diagonals again as the resonance is shifted inwards.

In conclusion, to make lithium MOT work at low magnetic field gradients, the detuning must be reduced according to Fig.(3.11), possibly compromising the number of atoms.

3.4.6 Compressing the MOT

According to the Doppler theory and as we have seen in the temperature measurements, the lowest temperatures are achieved for a small detuning, $\delta_{\text{theo}} = -\Gamma/2$ and $\delta_{\text{exp}} = -3\Gamma$, but limit the number of atoms. A cooling technique for lithium called compressed MOT (CMOT) has been developed by Ref. [31, 52]. It consists in loading a large number of atoms at large detuning and then ramping the detuning to $-\Gamma/2$ within several milliseconds. The detuning close to resonance enhances the losses and therefore the compression has to be done right before the transfer into the magnetic trap [31]. The intensity is simultaneously ramped down below the saturation intensity

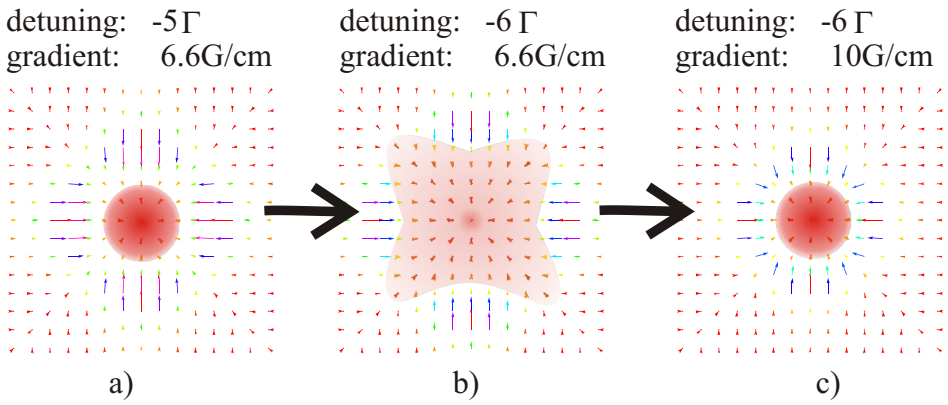

Figure 3.12: Simplified picture of the forces on the atoms in a MOT. The force field of a MOT is illustrated for different conditions. The MOT is surrounded in a), whereas increasing the detuning opens holes along the diagonals due to the finite beam size, as shown in b). To confine again the atoms, the gradient can be increased, c). For all figures, zero velocity is assumed to compute the force fields.

to minimize the losses and heating due to the increased scattering rate. In Fig.(3.13) we show that ramping the MOT detuning from -5Γ to -3Γ in 5ms does slightly reduce the width of the expanding cloud (after a TOF of 1ms). The ramp is, so far, implemented using a frequency shift of the MOT AOM, therefore, the intensity is lowered automatically due to the changing diffraction efficiency of the AOM.

Up to now, it is not possible to ramp the frequencies using the spectroscopy AOM, because of a changing (frequency dependent) offset on the lock-in signal. Apart from that, we do not know yet how crucial compressing of the lithium MOT will be when being mixed with a much larger sodium MOT, so no further attempts of compressing were done.

3.5 Magnetic Trapping

Trapped in a MOT, the atoms are being held mainly by the light forces. The magnetic field gradient only provides a position dependence to the optical molasses (2.1.3). The situation in the magnetic trap (MT) is different. There the potential is created by a steep magnetic field gradient. The transfer of *sodium* atoms into the MT is done by raising the magnetic field gradient to compensate the light forces at the moment when the laser light is switched off. The ramp-speed and magnitude of the gradient are optimized for best

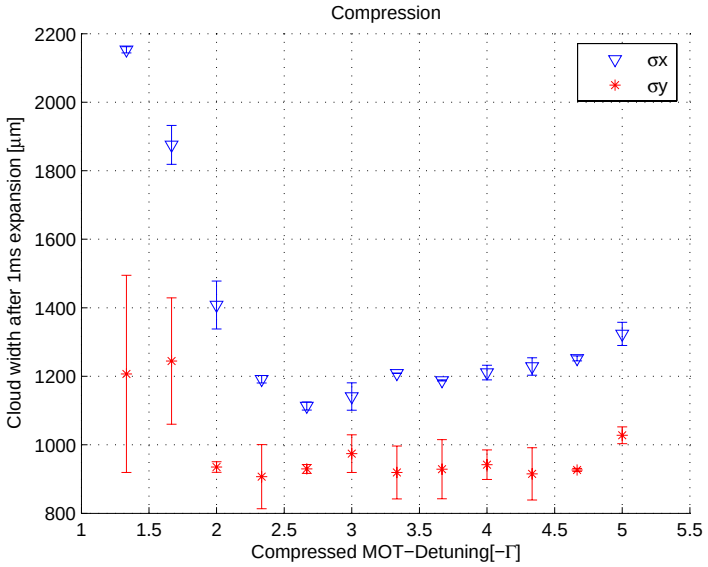

Figure 3.13: First attempts of the compressing of the MOT. The detuning of the MOT light is ramped from -5.5Γ to different values in 5ms. The width of the cloud after 1ms of free expansion is measured.

transfer of sodium. For lithium, after using the same sequence no atoms could be detected in the MT. Before we try to find out, what is the problem during the transfer, let us have a look on what states can be trapped in a MT.

3.5.1 Trappable ^{6}Li

Magnetically trappable, that is low-field seeking, states of ^{6}Li are $F = 3/2, m_\mathrm{F} = 3/2$, $F = 3/2, m_\mathrm{F} = 1/2$ and $F = 1/2, m_\mathrm{F} = -1/2$, which can be seen in the Breit-Rabi diagram Fig.(3.14). Due to a relatively weak hyperfine interaction, the nuclear spin decouples from the total angular momentum at a relatively low magnetic field. In the case of the $F = 1/2, m_\mathrm{F} = -1/2$ state this means that above $B = 27$G the state is high-field seeking and cannot be trapped in the MT. The trap depth for this state is limited to approximately 300μK. Considering the temperature of our MOT, most of the atoms in this state would be at a magnetic field above 27G and therefore accelerated outwards.

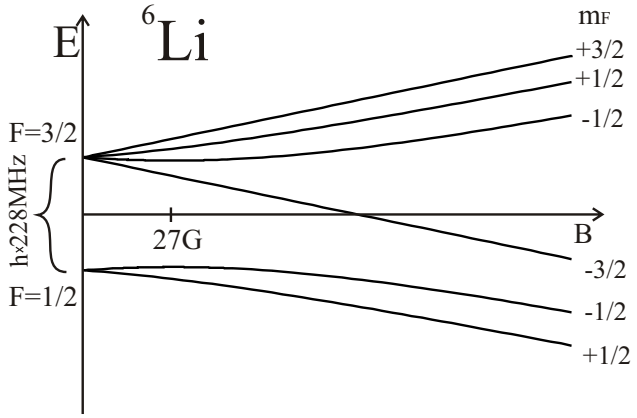

Figure 3.14: Breit-Rabi diagram for 6Li and the trappable states. $F = 1/2, m_{\mathrm{F}} = -1/2$ is low-field seeking for a magnetic field below 27G and high-field seeking for higher fields.

3.5.2 First Results

To ensure a maximal transfer efficiency into the MT, the $F = 3/2 \rightarrow F'$ (MOT) light is turned off prior to $F = 1/2 \rightarrow F'$ (repumper) pumping most of the atoms into the $F = 3/2$ ground state. Subsequently, the process of transferring into the MT is monitored by taking absorption images every 100μs.

The key to a first trapping of atoms in MT consisted in switching the light off *after* the gradient was ramped up to $B = 70$G/cm. The preliminary transfer efficiency for $F = 3/2$ atoms amounts only to 10% and it is also possible to load $F = 1/2$ atoms, however, merely 1% are trapped in the MT. It turns out that atoms in the MOT do not sit in the magnetic field zero, this is due to misaligned laser beams. By raising the gradient, the atoms sitting on the slope of the potential are given lots of energy allowing them to escape.

Atoms in $F = 3/2$ state can be detected after about 1s of holding in the MT. A main limiting factor is certainly the stray light since no mechanical shutters for laser light have been set up yet.

The transfer efficiency can be increased, when ensuring a better alignment of the MOT and the magnetic field zero. The loading sequence has to be optimized as well.

The major step ahead is the simultaneous operation of sodium and lithium MOTs and the transfer into the magnetic trap. An important question will be what lithium state can be trapped in MT in the presence of sodium:

the combination of $(F = 1, m_{\mathrm{F}} = -1)_{\mathrm{Na}}$ and $(F = 1/2, m_{\mathrm{F}} = -1/2)_{\mathrm{Li}}$ is stable against spin-exchange collisions, but thermalisation of lithium with sodium at $1mK$ may eventually spill out all of lithium over the 27G edge. Another possibility is to go for $(F = 3/2)_{Li}$ state, sympathetically cool below 50μK and then transfer the lithium atoms into the $F = 1/2$ state as was demonstrated by Ref. [32].

Chapter 4

Conclusion and Outlook

Polaron experiments require three main ingredients, a **medium**, an **impurity** and **interaction** between the medium and the impurity.

10^5 sodium atoms in the $F = 1, m_F = -1$ state at a temperature of 5μK were prepared in the course of this thesis. The bimodal momentum distribution and the anisotropic expansion indicate the emergence of a Bose-Einstein condensate, which is the first ingredient for coming polaron experiments.

The laser system for laser cooling of fermionic lithium-6 is the main achievement of the thesis (see Fig.(4.1)). A spectroscopy has been put into operation and the existing sodium setup has been modified to allow for simultaneous cooling and trapping of lithium and sodium. Within a few seconds, about 10^7 lithium atoms are loaded into the magneto-optical trap. The temperature of the trapped lithium amounts to 700μK to 1.5mK. The number of atoms is rather modest, compared to similar setups. But considering the role of lithium as impurity, which implies low density compared to the density of the medium, we ventured the next step. We are able to transfer $10^5 - 10^6$ lithium atoms into the magnetic trap.

The last ingredient

The interactions between lithium and sodium will become important when the two species are simultaneous transfered in to the magnetic trap. Sympathetic cooling of lithium relies on thermalisation with sodium, that is being evaporated.

The main interest of interactions arises as soon as degeneracy of sodium is reached. In order to tune the interactions with a homogeneous magnetic field, the ultracold atoms will be transfered in an optical dipole trap, described in the thesis of Raphael Scelle[44]. An additional optical dipole trap for lithium

will enable controlling of the lithium independently from the sodium. This opens various experimental possibilities. Oscillation frequencies of lithium will reveal polaronic properties. Self-localization of polarons may occur at high interaction strengths and could be detected by the change of momentum distribution. Furthermore, dragging lithium within the condensate at different velocities may give insight in superfluidity on a microscopic level.

Figure 4.1: Optics of the laser system for lithium.

Appendix A

Spectroscopy for Lithium

The implementation of spectroscopy locking of the laser is explained step-by-step. Several obstacles have been overcome, namely the noisy signal, outgasing heatpipe and coating of the windows with lithium.

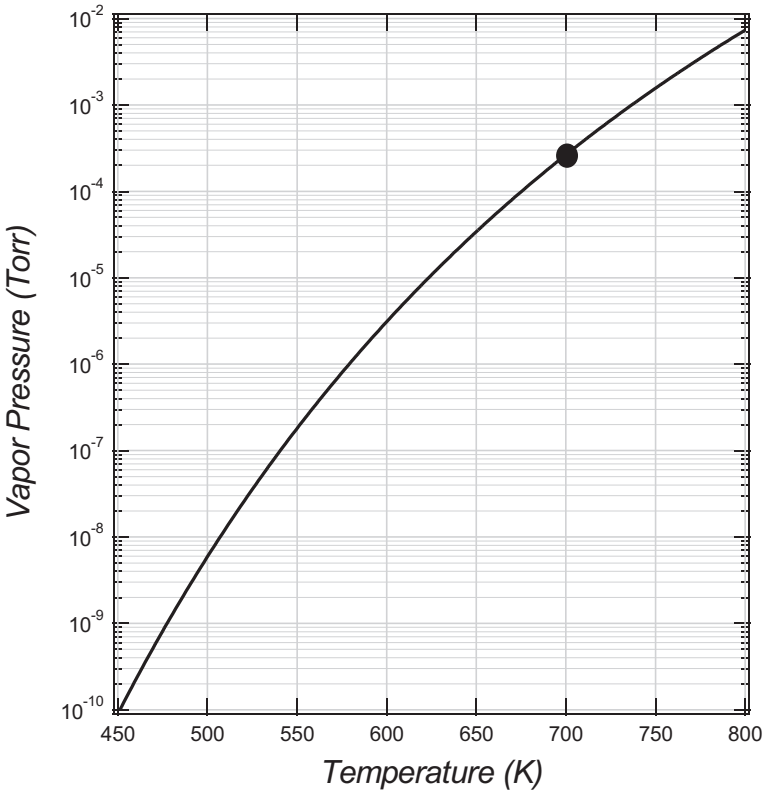

Figure A.1: Vapor pressure of lithium as a function of temperature.

A.1 First spectroscopy cell

The vapor pressure of lithium is shown in Fig.(A.1). Compared to sodium, the vapor pressure of lithium four orders of magnitude lower! Depending on the design of the spectroscopy cell, temperatures up to 380°C are required to obtain an absorption signal of several percent[53]. Unfortunately, glass undergoes chemical reaction with hot lithium gas and becomes opaque. A special heat pipe has to be built. Fig.(A.2) shows our first spectroscopy cell, it features a mesh inside the steel tube to prevent lithium from reaching the windows. Moreover, the outer ends are always at room temperature due to the low heat conductance of steel and the large aluminum blocks used as heat dissipators.

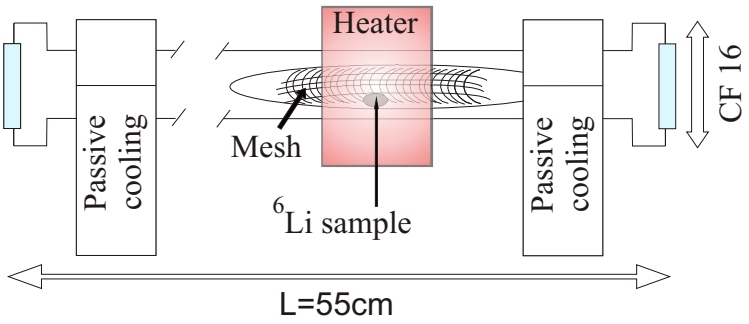

Figure A.2: The first spectroscopy cell. The mesh shall reduce the mean free pass of lithium atoms, reducing the contact of lithium to the glass windows.

A.2 Doppler Spectroscopy

To test the heat pipe a probe beam with 1mW[1] was sent used. The wavelength of the laser was scanned between 670.950nm and 671.0nm. As expected, two absorption features were detected: absorption at 670.977nm and 670.992nm, corresponding to D2 and D1 lines. Fig.(A.3) shows the scan over the D2 line. Due to the Doppler broadening of atoms at 330°C, the line appears visibly broader, than the natural line width of $2\pi \times 5.87$MHz. The velocities of atoms moving along the beam are distributed according to the Maxwell-Boltzmann distribution, which is in one dimension a Gaussian. The determined width of 2GHz fits well to the expected Doppler broadening at $T = 330$°C given by: $\Delta = (\omega_0/c)\sqrt{8k_B T ln2/m}$ [54].

[1]First spectroscopy measurements were performed with a dye laser.

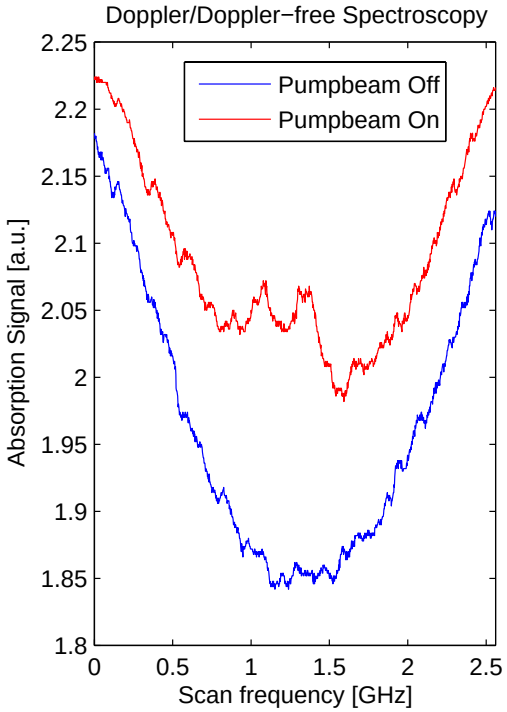

Figure A.3: Doppler and Doppler-free spectroscopy. Intensity fluctuations of the laser completely overcast the interesting features, therefore, both graphs are averages of 16 scans.

A.3 Doppler-free spectroscopy

To extract the natural transition line out of the Doppler-valley we use an additional, counterpropagating laser beam, see Fig.(A.4,a). This so-called pump beam, having the same frequency ω as the probe beam but a higher intensity, excites atoms resonantly at $\omega = \omega_0 + kv$. The probe beam is absorbed by atoms resonant at $\omega = \omega_0 - kv$. Only atoms with $v = 0$ in the directions of the beams see both beams at the same time, this weakens the absorption of the probe beam, as atoms are likely to be excited by the stronger pump beam [54]. The resulting signal shown in Fig.(A.3) has a dip in the center. The signal is very noisy and requires averaging over 16 scans to see the relatively small dip. In order to amplify and clean the signal a lock-in amplifier is used.

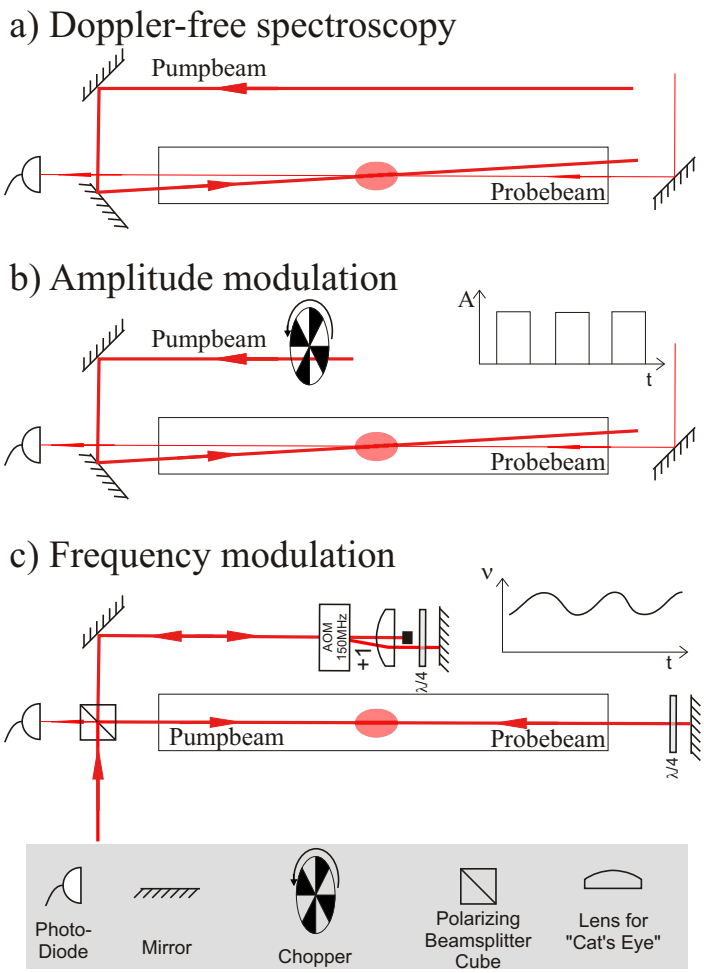

Figure A.4: Different spectroscopy setups. In a) the first setup is depicted. Because of the strong noise, amplitude modulation as shown in b) was introduced by using a chopper. Final set-up for spectroscopy locking using an AOM for frequency modulation is illustrated in c). The probe beam is the retro-reflected pump beam.

A.4 Amplitude modulation

A.4.1 Clean signal

A lock-in amplifier[2] is basically a narrow bandpass filter combined with an amplifier. It extracts and amplifies a signal at a defined frequency while

[2]We are using Femto LIA-BV-150-H

suppressing all other frequencies. We can use a chopper to modulate our pump beam with a square waveform (see Fig.(A.4,b)). The modulation frequency $\omega_m = 2\pi \times 1\text{kHz}$ is chosen to be much larger than the frequency $\omega_s = 2\pi \times 10\text{Hz}$ at which the laser is scanned. The absorption signal U_a of the probe beam is therefore also modulated when the laser scans over the dip. Since $\omega_s \ll \omega_m$ we can assume the laser frequency ν_{Laser} to be constant at the timescale of the modulation:

$$U_a(\nu_{\text{Laser}}) \overset{\text{modulation}}{\rightarrow} U_a(\nu_{\text{Laser}})\Theta_{sw}(\omega_m t) \tag{A.1}$$

The square waveform Θ_{sw} can be expanded to

$$\Theta_{sw}(\omega_m t) = \Sigma(a_n cos(n\omega_m t) + b_n sin(n\omega_m t) \tag{A.2}$$

The lock-in amplifier is fed with the modulated U_a and a reference signal, providing ω_m. It mixes the input with a $cos(\omega_m t + \phi)$[3], giving:

$$U_a(\nu_{\text{Laser}})(\Sigma(cos(\omega_m t + \phi)a_n cos(n\omega_m t) + cos(\omega_m t + \phi)b_n sin(n\omega_m t)) \tag{A.3}$$

Using trigonometric identities [4] , we end up with one time-independent term and many oscillating terms. After mixing, the signal goes through a low-pass filter, which corresponds to a time integration. The output can be written as:

$$U_{Out} = \frac{1}{T}\int_0^T U_a(\nu_{\text{Laser}})\,(cos(\phi) + \Sigma(cos(n\omega_m t + \phi) + \ldots))\,^{5} \tag{A.4}$$

The integration time T can be set such that $T >> 1/\omega_m$, which leads to averaging over all oscillating terms, leaving us an output proportional to the absorption signal.

$$U_{\text{Out}} \propto U_a(\nu_{\text{Laser}})cos(\phi) \tag{A.5}$$

It means, that what we get out is the same as we put in, except for the modulation which is gone. For a scheme see Fig.(A.5).

[3] ϕ is the phase between the input signal and the mixing signal.

[4] $cos(\alpha)cos(\beta) = 1/2(cos(\alpha - \beta) + cos(\alpha + \beta)$ and $cos(\alpha)sin(\beta) = 1/2(sin(\beta - \alpha) + sin(\beta + \alpha)$ [55].

[5] In order to keep the formula simple, constants and terms with $sin(n\omega_m t + \phi)$ have been omitted, since they do not play a role for the working principle of the lock-in technique.

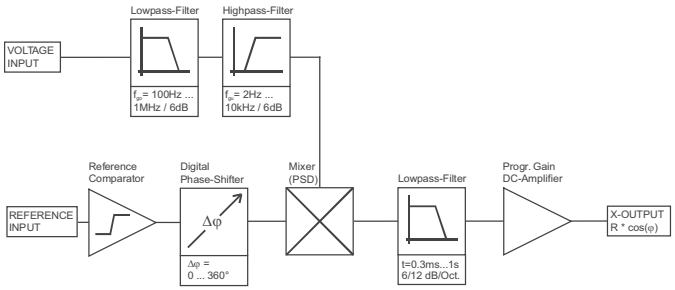

Figure A.5: Simplified schematic of a lock-in amplifier. The input signal is pre-filtered with the bandpass filter consisting of a lowpass and highpass filter. The phase sensitive detector (PSD) mixes the input signal with a reference cosine. The last low-pass filter eliminates oscillating high frequency components.

A.4.2 Noisy Signal

So far, we have considered a signal without noise. The noise on a signal can be described as a function with a broad frequency spectrum, that is added to our spectroscopy signal:

$$U_a(\nu_{\text{Laser}}) \overset{noise}{\rightarrow} U_a(\nu_{\text{Laser}}) + \int A_{\text{Noise}}(\omega) cos(\omega t) d\omega \tag{A.6}$$

with $A_{\text{Noise}}(\omega)$ as an arbitrary amplitude of the noise. Mixing the noise term with $cos(\omega_m t + \phi)$ and averaging over the time T leads to:

$$\begin{aligned} U_{\text{Out}} \propto & U_a(\nu_{\text{Laser}}) cos(\phi) \\ & + \frac{1}{T} \int_0^T dt \int d\omega A_{\text{Noise}}(\omega) \left(cos((\omega_m - \omega)t + \phi) + cos((\omega_m + \omega)t + \phi) \right) \end{aligned} \tag{A.7}$$

Now, only noise with frequencies $(\omega_m - \omega) < \frac{1}{T}$ 'survives' the averaging, while all other noise contributes only with a time-independent offset. The time constant T can be chosen in the range of $0.3\text{ms} - 1\text{s}$ and stands for the inverse bandwidth of the band pass. On the other hand, it is important, that the averaging time T is much shorter than the timescale of interesting features in our spectroscopy.

To sum up, in order to eliminate the noise from the signal we mix the input with a cosine and average out contributions of all frequencies but one, to keep the sought signal from averaging we modulate it with the reference frequency. The phase ϕ can be adjusted to maximum output[56].

A.4.3 Results

In Fig.(A.6,a) both photodiode and lock-in amplified absorption signal are shown. The width of the Doppler-free peak amounts to several hundred MHz, which is much broader than the expected line width of $2\pi \times 6$MHz. There are two possible mechanism responsible for line broadening: power broadening and pressure broadening. Power broadening can be directly extracted out of the scattering rate. The power-broadened line width of the transition is given by $\Gamma' = \Gamma\sqrt{1+S_0}$ [23]. Since the intensity in the probe beam is less than the saturation intensity, we should have almost no broadening due to power.

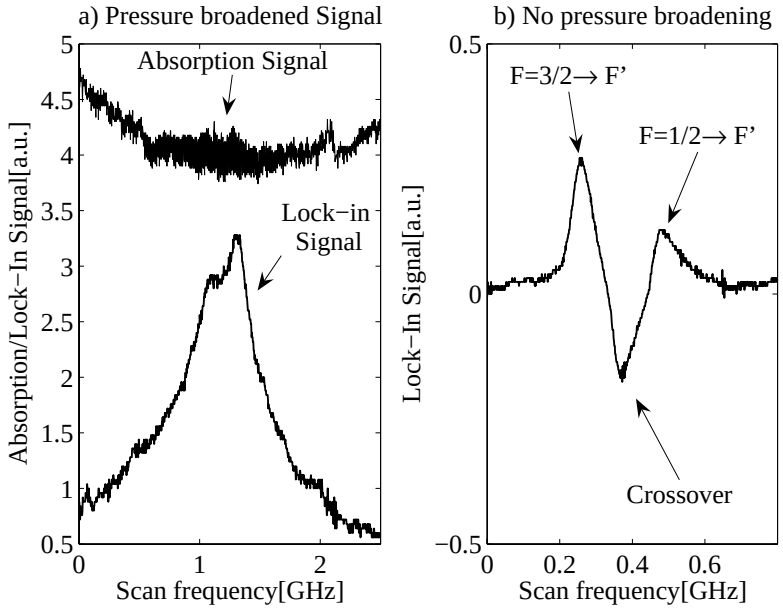

Figure A.6: Background pressure of several mbar broadened the hyperfine lines. In a), the unfiltered absorption signal shows 50Hz noise at the resonance coming from the ac-heater and thus created ac-Zeeman shift. Figure b) shows the expected hyperfine structure lines and the cross-over feature.

Pressure broadening results from potentials of nearby particles that shift the energy and thus the frequency of the transition. The width Δ_B of of the broadening depends basically on the pressure, being in the order of magnitude of $\Delta_B \approx 10$MHz/mbar [54]. Indeed, the two hyperfine lines as well as their crossover became visible as soon as the pressure in the heat pipe was reduced below 0.2mbar, as shown in Fig.(A.6,b).

A.5 Frequency modulation

The crossover peak in the spectroscopy is just an artifact sitting right between the two hyperfine lines at the frequency $\omega_c = \omega_{F=1/2} - \omega_{F=3/2}$. When the pump beam scans over ω_c, it is resonant with $F = 3/2$ atoms moving towards the beam at the velocity of $v_c = (\omega_c - \omega_{F=3/2})/k$. The pump beam optically pumps this velocity class into the $F = 1/2$ state, while at the same time, atoms in $F = 1/2$ with v_c are in resonance with the probe beam. The high population of $F = 1/2$ state at v_c gives rise to an enhanced absorption of the probe beam, hence a negative crossover peak. Since the crossover is the most pronounced feature in the spectroscopy, we lock our laser to it.

The spectroscopy signal itself cannot be used as a setpoint for the laser frequency, since we want to lock at the top of the peak and drifting of the laser in both direction would give a positive feedback to a controller. However, for small deviations, the *derivative* of the peak is linear and can be directly used as an error signal.

We use the lock-in amplifier to get the derivative of the signal. At the same time, frequency modulations yields the same narrow band filter, hence reduces the noise. The frequency is modulated using an acousto-optical modulator (AOM) in a double pass configuration. The first order maximum has a frequency shift of $\delta\nu = 2 \times (150\text{MHz} + \Delta cos(\omega_m t))$, with $\Delta \approx 5\text{MHz}$ and $\omega_m \approx 20\text{kHz}$ provided by a frequency generator.

$$U_a(\nu_{\text{Laser}}) \overset{modulation}{\rightarrow} U_a(\nu_{Laser} + \delta\nu)) = U_a(\nu + \Delta cos(\omega_m t)) \tag{A.8}$$

For small modulation amplitudes the signal can be expanded as:

$$U_a(\nu + \delta\nu) \approx U_a(\nu) + \frac{dU_a(\nu)}{d\nu}\delta\nu \tag{A.9}$$

Mixing the input signal with $cos(\omega_m t + \phi)$ leads to a constant term $\frac{dU_a(\nu)}{d\nu}\Delta cos(\phi)$, directly proportional to the derivative, while all other terms have oscillating factors:

$$\frac{1}{2}\frac{dU_a(\nu)}{d\nu}\Delta cos(\phi) + U_a(\nu)cos(\omega_m t + \phi) + \frac{1}{2}\frac{dU_a(\nu)}{d\nu}\Delta cos(2\omega_m t + \phi) \tag{A.10}$$

Again, a low-pass filter averages out the oscillating terms. The output of the lock-in amplifier in Fig.(A.7) is now the derivative of the spectroscopy signal. The largest slope corresponds to the crossover peak. We can lock a controller on the zero-crossing of the derivative. Spectroscopy locking of the laser has a long-time stability of about a day.

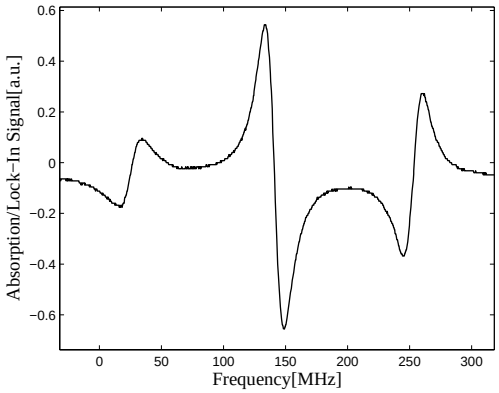

Figure A.7: Frequency modulated spectroscopy. The largest slope is used for locking of the laser.

A.6 A new spectroscopy cell

Given the mentioned difficulties, a new spectroscopy cell was built, see Fig.(3.2) and Fig.(A.8). Several improvements were implemented. The evacuation tube was welded directly on the heat pipe, instead of using Swagelok fittings. Since refilling turned out to be problematic, the mesh inside was left out. Besides, outgassing problems were probably related to the large surface of the mesh. Instead, a small lithium crucible of steel has been manufactured. The boat facilitates refilling of the heat pipe and keeps lithium localized.

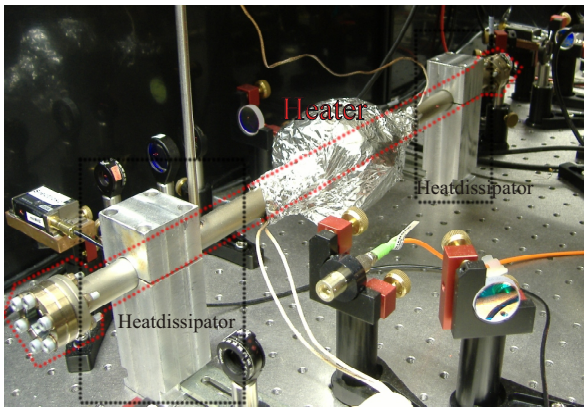

Figure A.8: The figure shows the new spectroscopy cell in action. The aluminum blocks dissipate the heat and keep the outer ends of the heat pipe at room temperature.

Appendix B

Lithium transition strengths and constants

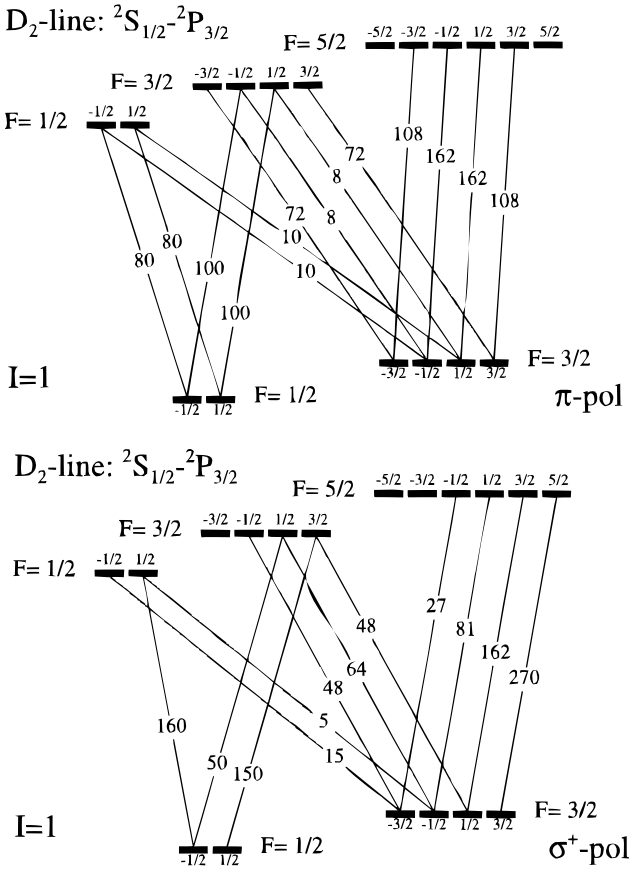

Figure B.1: Transition strengths for lithium-6. Taken from Ref.[23]

Fundamental Constants

Quantity	Symbol	Value	Unit
Speed of light	c	$2.99792458 \cdot 10^{8}$	m/s
Boltzmann Constant	k_B	$1.3806503(24) \cdot 10^{-23}$	J/K
Planck Constant	h	$6.62606876(52) \cdot 10^{-34}$	Js
	$h/2\pi$	$1.054571596(82) \cdot 10^{-34}$	Js

^{6}Lithium data and D2 line properties [57]			
Mass	m	$9.9883414 \cdot 10^{-27}$	kg
Wavelength	λ	670.977338	nm
Frequency	ω_0	$2\pi\times$ 446.799677	THz
Saturation Intensity	I_{S}	2.54	mW/cm^2
Natural Linewidth	Γ	$2\pi \times 5.8724$	MHz
Doppler Temperature	T_{D}	140.915	μK

Appendix C

Interlock System

The MOT-coils as well the coils of the Zeeman slower are steadily cooled with water that dissipates the produced heat[26, 41]. If, for some reason, the cooling circuit is interrupted while the coils are in operation, the coils and the whole experimental setup may suffer heavy damage due to the overheating of the coils.

In the course of this thesis an interlock system to prevent overheating of the coils has been designed and tested. The idea is to monitor the temperature of the coils and to cut the current through the coils when the temperature exceeds a defined value.

Fig.(C.1) illustrates a simplified schematic of the interlock circuit. Simplified means that it only contains the elements necessary to understand the working principle. The temperature sensors are resistors, with a resistance depending on their temperature. We are using the type KTY, their resistance increases with higher temperature. The KTY-sensors are attached pair-wise on different positions on the coils.

The resistance of one sensor (R1) is compared to a reference resistance of (R2), which corresponds to a threshold temperature. This is done by comparing the voltage drop over R1 and R2 using a comparator IC (LM339). The output of the comparator goes from low to high when the resistance of the sensor becomes larger than that of the reference. A yellow LED lights up in this case.

At the same time the other sensor (R3) also exceeds the reference threshold (R4). The outputs of both comparators are fed into an AND-gate. When both outputs change to high, the output of the AND-gate also changes to high. This is the signal that should switch off the current through the coils. To this end, a relay 'closes' and switches the control voltage to a value corresponding to zero-current. However, if the temperature decreases below the threshold, the relay 'opens' again, leading to renewed heating. Therefore,

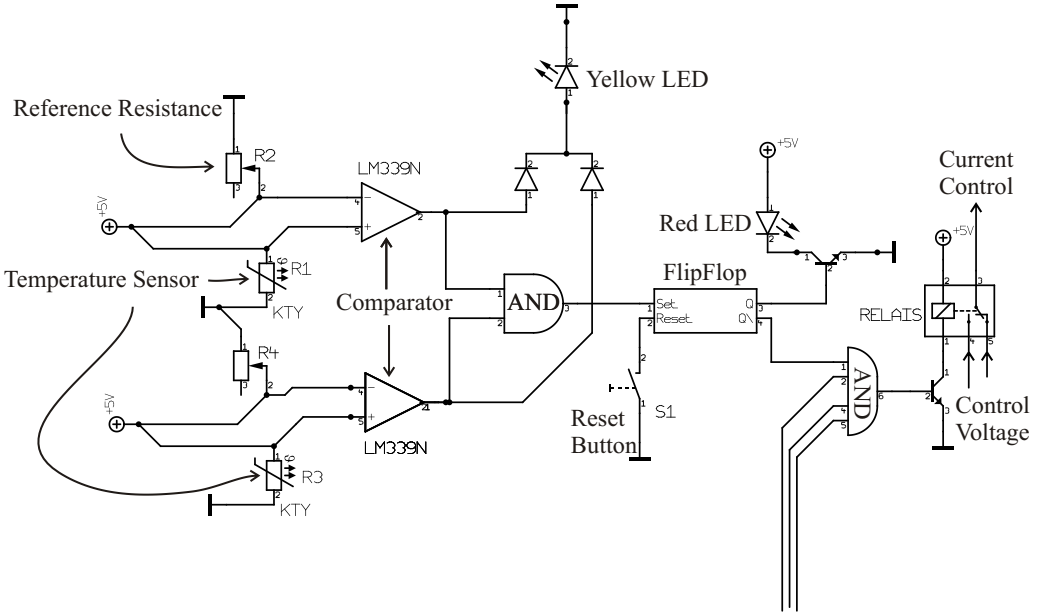

Figure C.1: Simplified schematic of the interlock circuit.

we use a flipflop (SR latch), to 'memorize' the crossing of the threshold. Even when the AND-gate changes to low, the output of the flipflop does not change. At the same time a red LED is lit to alert the people in the lab. Once the defect is fixed, the flipflop is reseted by disconnecting the reset port from the ground via a button.

At normal operation, the coil of the relay is constantly conducting current. It means that in case of an electricity failure affecting the interlock circuit, the relay automatically closes and inhibits uncontrolled operation of the coils.

Since four pairs of temperature sensors are used to monitor the MOT-coils, the circuit shown in Fig.(C.1) is reproduced four times. All flipflop outputs $\bar{Q}$ are fed in to a four-input AND gate, which ensures that each pair of sensors can independently switch off the current.

Anhang D

Danksagung

Ich möchte gern allen danken, die mich unterstützt haben. Mein besonderer Dank gilt:

- Prof. Markus K. Oberthaler, der mich in das NaLi Experiment aufgenommen und diese Arbeit ermöglicht hat. Vor allem seine Begeisterung für kleine (z.B. Koppeln von AOMs) sowie für große Dinge (Polaronen, Quark-Gluon Plasma, etc) hat mich angesteckt und die gesamte Zeit begleitet.

- Juniorprof. Selim Jochim nicht nur für die Begutachtung dieser Arbeit, sondern auch für die regelmässigen Pizza-Abende mit seiner Gruppe.

- Jens Appmeier für die vielen wertvollen Disskussionen und das kritische Korrekturlesen dieser Arbeit.

- dem NaLi-Team für die schöne Zeit im Labor und ausserhalb. Fabienne und Bernhard danke ich ebenfalls für das Korrekturlesen meiner Arbeit.

- allen Mitgliedern der Matterwave Gruppe für die angenehme Atmosphäre und die vielen Aktivitäten wie Beach-en, Grillen, Stammtisch und Feiern.

- meinen Eltern, die das Studium ermöglicht haben und allen Freunden, die die Studienzeit viel zu kurz erscheinen lassen haben.

- Kathrin für das Mitmachen bei all' dem Physiker-Quatsch ;)

Bibliography

[1] David J. Miller. A quasi-political Explanation of the Higgs Boson; for Mr Waldegrave, UK Science Minister. `http://www.hep.ucl.ac.uk/~djm/higgsa.html`, 1993.

[2] K.B. Davis, M.-O. Mewes, M.R. Andrews, N.J. van Druten, D.S. Durfee, D.M. Kurn, and W. Ketterle. Bose-Einstein condensation in a gas of sodium atoms. *Phys.Rev.Lett.*, **75**:3969, 1995.

[3] M.H. Anderson, J.R. Ensher, M.R. Matthews, C.E. Wieman, and E.A.Cornell. Observation of Bose-Einstein condensation in a dilute atomic vapor. *Science*, **269**:198, 1995.

[4] C.C. Bradley, C.A. Sackett, J.J. Tollett, and R.G. Hulet. Evidence of Bose-Einstein condensation in an atomic gas with attractive interactions. *Phys.Rev.Lett.*, **75**:1687, 1995.

[5] M. R. Andrews, C. G. Townsend, H. j. Miesner, D. S. Durfee, D. M. Kurn, and W. Ketterle. Observation of Interference Between Two Bose Condensates. *Science*, **275**(5300):637–641, 1997.

[6] Michael Albiez, Rudolf Gati, Jonas Fölling, Stefan Hunsmann, Matteo Cristiani, and Markus K. Oberthaler. Direct Observation of Tunneling and Nonlinear Self-Trapping in a Single Bosonic Josephson Junction. *Phys. Rev. Lett.*, **95**(1):010402, Jun 2005.

[7] Markus Greiner, Olaf Mandel, Tilman Esslinger, Theodor W. Hänsch, and Immanuel Bloch. Quantum phase transition from a superfluid to a Mott insulator in a gas of ultracold atoms. *Nature*, **415**(6867):39–44, January 2002.

[8] W. Ketterle. Observation of Feshbach resonances in a Bose-Einstein condensate. *Nature*, **392**, 1998.

[9] C. A. Regal, M. Greiner, and D. S. Jin. Observation of Resonance Condensation of Fermionic Atom Pairs. *Phys. Rev. Lett.*, **92**(4):040403, Jan 2004.

[10] M. Zwierlein, J. Abo-Shaeer, A. Schirotzek, C. Schunck, and W. Ketterle. Vortices and Superfluidity in a Strongly Interacting Fermi Gas, May 2005.

[11] J. Bardeen, L. N. Cooper, and J. R. Schrieffer. Microscopic Theory of Superconductivity. *Physical Review*, **106**(1):162–164, 1957.

[12] Andre Schirotzek, Cheng-Hsun Wu, Ariel Sommer, and Martin W. Zwierlein. Observation of Fermi Polarons in a Tunable Fermi Liquid of Ultracold Atoms, 2009.

[13] Kenneth Günter, Thilo Stöferle, Henning Moritz, Michael Köhl, and Tilman Esslinger. Bose-Fermi Mixtures in a Three-Dimensional Optical Lattice. *Physical Review Letters*, **96**(18):180402, 2006.

[14] S. Ospelkaus, C. Ospelkaus, L. Humbert, K. Sengstock, and K. Bongs. Tuning of Heteronuclear Interactions in a Degenerate Fermi-Bose Mixture. *Physical Review Letters*, **97**(12):120403, 2006.

[15] A. Einstein. Quantentheorie des einatomigen idealen Gases. *Sitzungsberichte der Königlich-Preußischen Akademie der Wissenschaften*, **1**:3, 1925.

[16] Grigori Astrakharchik. Properties of a Bose Gas in the Presence of Disorder, 2001.

[17] Lev Pitaevskii and Sandro Stringari. Bose-Einstein Condensation. Oxford Science Publications, 2002.

[18] Fernando M. Cucchietti and Eddy Timmermans. Small polarons in dilute gas Bose-Einstein condensates, 2006.

[19] C. A. Stan, M. W. Zwierlein, C. H. Schunck, S. M. F. Raupach, and W. Ketterle. Observation of Feshbach Resonances between Two Different Atomic Species. *Phys. Rev. Lett.*, **93**(14):143001, Sep 2004.

[20] Ryan M. Kalas and D. Blume. Interaction-Induced Localization of an Impurity in a Trapped Bose Condensate, 2005.

[21] L. J. LeBlanc and J. H. Thywissen. Species-specific optical lattices. *Physical Review A (Atomic, Molecular, and Optical Physics)*, **75**(5):053612, 2007.

[22] Martin Bruderer, Alexander Klein, Stephen R. Clark, and Dieter Jaksch. Polaron physics in optical lattices. *Physical Review A (Atomic, Molecular, and Optical Physics)*, **76**(1):011605, 2007.

[23] Peter van der Straten Harold J. Metcalf. Laser Cooling and Trapping. Springer-Verlag, 2002.

[24] Karolina Brugger. Experimente mit mikroskopischen atomoptischen Elementen. PHD thesis, Universität Heidelberg, 2004.

[25] William D. Phillips and Harold Metcalf. Laser Deceleration of an Atomic Beam. *Phys. Rev. Lett.*, **48**(9):596–599, Mar 1982.

[26] Jan Krieger. Zeeman-Slower und Experientsteuerung für das NaLi-Experiment, 2008.

[27] E. M. Lifshitz and L. D. Landau. Quantum Mechanics: Non-Relativistic Theory, 6th Edition: Volume 3 (Course of Theoretical Physics). FIZMATLIT, 2004.

[28] E. Raab, M. Prentiss, A. Cable, S. Chu, and D. Pritchard. Trapping of neutral-sodium atoms with radiation pressure. *Phy.Rev.Lett.*, **59**:2631, 1987.

[29] A. Cable, M. Prentiss, and N. P. Bigelow. Observations of sodium atoms in a magnetic molasses trap loaded by a continuous uncooled source. *Opt. Lett.*, **15**(9):507–509, 1990.

[30] P. S. Julienne and Jacques Vigué. Cold collisions of ground- and excited-state alkali-metal atoms. *Phys. Rev. A*, **44**(7):4464–4485, Oct 1991.

[31] Marc-Oliver Mewes, Gabriele Ferrari, Florian Schreck, Alice Sinatra, and Christophe Salomon. Simultaneous magneto-optical trapping of two lithium isotopes. *Phys. Rev. A*, **61**(1):011403, Dec 1999.

[32] Z. Hadzibabic, C. A. Stan, K. Dieckmann, S. Gupta, M. W. Zwierlein, A. Görlitz, and W. Ketterle. Two-Species Mixture of Quantum Degenerate Bose and Fermi Gases. *Phys. Rev. Lett.*, **88**(16):160401, Apr 2002.

[33] Marc Repp. Aufbau einer Vakuumapparatur für Experimente mit ultrakalten fermionischen und bosonischen Quantengasen, 2007.

[34] Stefan Weis. Setup of a laser system for ultracold sodium- Towards a degenerate gas of ultracold fermions, 2007.

[35] W. Ketterle, K.B. Davis, M.A. Joffe, A. Martin, and David E. Pritchard. High densities of cold atoms in a dark spontaneous-force optical trap. *Phys.Rev.Lett*, **70**:2253, 1993.

[36] T. Walker, D. Sesko, and C Wieman. Collective behaviour of optically trapped neutral atoms. *Phys.Rev.Lett.*, page 408, 1990.

[37] John David Jackson. Classical Electrodynamics. John Wiley & Sons, Inc., 1962.

[38] A.L. Migdall, J.V. Prodan, and W.D. Phillips. First observation of magnetically trapped neutral atoms. *Phys.Rev.Lett*, **54**:2596, 1985.

[39] Z. Hadzibabic, S. Gupta, C. A. Stan, C. H. Schunck, M. W. Zwierlein, K. Dieckmann, and W. Ketterle. Fifty-fold improvement in the number of quantum degenerate fermionic atoms. *Physical Review Letters*, **91**:160401, 2003.

[40] K.B. Davis, M.-O. Mewes, M.A. Joffe, M.R. Andrews, and W. Ketterle. Evaporative cooling of sodium atoms. *Phys.Rev.Lett.*, **74**:5202, 1995.

[41] Anton Piccardo-Selg. Degenerate Quantum Gases: Towards Bose-Einstein Condensation of Sodium, 2008.

[42] W. Petrich, M.H. Anderson, J.R. Ensher, and Eric Cornell. Stable, Tightly confining magnetic trap for evaporative cooling of neutral atoms. *Phys.Rev.Lett.*, **74**:3352, 1995.

[43] Rudolf Grimm, Matthias Weidemüller, and Yurii B. Ovchinnikov. Optical dipole traps for neutral atoms, Feb 1999.

[44] Raphael Scelle. Diploma thesis, 2009.

[45] K.M.R. van der Stam, E.D. van Ooijen, R. Meppelink, J.M. Vogels, and P. van der Straten. Large atom number Bose-Einstein condensate of sodium. *Review of Scientific Instuments*, **68**:013102, 2007.

[46] W. Ketterle, D. S. Durfee, and D. M. Stamper-Kurn. Making, probing and understanding Bose-Einstein condensates. In *Bose-Einstein condensation in atomic gases*, pages 67–176, 1999.

[47] H. Smith and C.J. Pethick. Bose-Einstein condensate in dilute gases. Cambridge Universtiy Press, 2002.

[48] K.B. Davis, M.-O. Mewes, and W. Ketterle. An analytical model for evaporative cooling of atoms. *Appl.Phys.B*, **60**:155, 1995.

[49] U. Schünemann, H. Engler, M. Zielonkowski, M. Weidemüller, and R. Grimm. Magneto-optic trapping of lithium using semiconductor lasers. *Optics Communications*, **158**:263–273, 1998.

[50] L. Ricci, M. Weidemüller, T. Esslinger, A. Hemmerich, C. Zimmermann, V. Vuletic, W. König, and T. W. Hänsch. A compact grating-stabilized diode laser system for atomic physics. *Optics Communications*, **117**(5-6):541–549, June 1995.

[51] Bernhard Huber. Diploma thesis, 2009.

[52] Selim Jochim. Bose-Einstein Condensation of Molecules. PHD thesis, Universität Innsbruck, 2004.

[53] Gang Xu. Manipulation and Quantum Control of Ultracold Atoms and Molecules for Precision Measurements. PHD thesis, The University of Texas at Austin, 2001.

[54] W. Demtröder. Experimentalphysik 3 - Atome, Moleküle und Festkörper, volume 3. Springer.

[55] Ilja N. Bronstein, Konstantin A. Semendjajew, and Gerhard Musiol. Taschenbuch der Mathematik. Deutsch (Harri).

[56] Paul Horowitz and Winfield. Hill. The art of electronics / Paul Horowitz, Winfield Hill. Cambridge University Press, Cambridge [England] :, 2nd ed. edition, 1989.

[57] Michael E. Gehm. Properties of 6Li. `http://www.phy.duke.edu/research/photon/qoptics/techdocs/pdf/PropertiesOfLi.pdf`, 2003.

Erklärung:

Ich versichere, dass ich diese Arbeit selbstständig verfasst und keine anderen als die angegebenen Quellen und Hilfsmittel benutzt habe.

Heidelberg, den _____ _____

Unterschrift